RESEARCH ARTICLE

eIF2A-knockout mice reveal decreased life span and metabolic syndrome

Richard Anderson[1] | Anchal Agarwal[1] | Arnab Ghosh[1] | Bo-Jhih Guan[2] |
Jackson Casteel[1] | Nina Dvorina[3] | William M. Baldwin 3rd[3] | Barsanjit Mazumder[1] |
Taras Y. Nazarko[4] | William C. Merrick[5] | David A. Buchner[2,5] | Maria Hatzoglou[2] |
Roman V. Kondratov[1] | Anton A. Komar[1,5]

[1]Center for Gene Regulation in Health and Disease, Department of Biological, Geological and Environmental Sciences, Cleveland State University, Cleveland, Ohio, USA

[2]Department of Genetics and Genome Sciences, Case Western Reserve University School of Medicine, Cleveland, Ohio, USA

[3]Department of Inflammation and Immunity, Cleveland Clinic Lerner College of Medicine, Cleveland, Ohio, USA

[4]Department of Biology, Georgia State University, Atlanta, Georgia, USA

[5]Department of Biochemistry, Case Western Reserve University School of Medicine, Cleveland, Ohio, USA

Correspondence
Anton A. Komar, Center for Gene Regulation in Health and Disease and Department of Biological Geological and Environmental Sciences, Cleveland State University, Cleveland, OH 44115, USA.
Email: a.komar@csuohio.edu

Abstract

Eukaryotic initiation factor 2A (eIF2A) is a 65 kDa protein that functions in minor initiation pathways, which affect the translation of only a subset of messenger ribonucleic acid (mRNAs), such as internal ribosome entry site (IRES)-containing mRNAs and/or mRNAs harboring upstream near cognate/non-AUG start codons. These non-canonical initiation events are important for regulation of protein synthesis during cellular development and/or the integrated stress response. Selective eIF2A knockdown in cellular systems significantly inhibits

Abbreviations: 4EBP1/2, eIF4E-binding proteins 1 and 2; ACACA, acetyl-CoA carboxylase; ACLY, ATP citrate lyase; ANOVA, analysis of variance; ATF, activating transcription factor; ATGL, adipose triglyceride lipase; ATP, adenosine-5′-triphosphate; BAT, brown adipose tissue; BCA, bicinchoninic acid; BiP, binding immunoglobulin protein; BSA, bovine serum albumin; CD, cluster of differentiation; CHOP, CCAAT enhancer binding protein homologous protein; CRP, C-reactive protein; DAB, 3,3′-diaminobenzidine; DENR, density regulated protein; DMEM, Dulbecco's modified eagle medium; DMSO, dimethyl sulfoxide; DNA, deoxyribonucleic acid; EDTA, ethylenediaminetetraacetic acid; eIF, eukaryotic initiation factor; ELISA, enzyme-linked immunosorbent assay; ER, endoplasmic reticulum; ERK1/2, extracellular signal-regulated kinase 1/2; FASN, fatty acid synthase; FBS, fetal bovine serum; GADD34, growth arrest and DNA damage-inducible protein 34; GCN2, general control non-derepressible 2; GTP, guanosine-5′-triphosphate; GTT, glucose tolerance test; H&E, hematoxylin and eosin (staining); HF, high-fat; HRI, heme-regulated eIF2α kinase; HSL, hormone-sensitive lipase; IACUC, Institutional Animal Care and Use Committee; ICAM-1, intercellular adhesion molecule 1; IGFBP-2, insulin-like growth factor-binding protein 2; IGFBP-6, insulin-like growth factor-binding protein 6; IGF-II, insulin-like growth factor 2; IRES, internal ribosome entry site; ISR, integrated stress response; ITT, insulin tolerance test; KO, knockout; LC3, microtubule associated protein 1 light chain 3 beta; LCN2, lipocalin-2; MEF, mouse embryonic fibroblast; Met-tRNAi, methionyl-tRNAi; MHC, major histocompatibility complex; mRNA, messenger ribonucleic acid; NGAL, neutrophil gelatinase-associated lipocalin; PAS, power analysis software; PBS, phosphate buffer saline; PCR, Polymerase Chain Reaction; PERK, PKR-like ER kinase; PKR, double-stranded RNA-dependent protein kinase; PLIN2, perilipin 2; PPARγ, peroxisome proliferator-activated receptor γ; RIPA, radioimmunoprecipitation assay; RNA, ribonucleic acid; rRNA, ribosomal ribonucleic acid; RT, reverse transcription; SDS, sodium dodecyl sulfate; SEM, standard error of the mean; SQSTM1, sequestosome 1 (p62); TC, ternary complex; Tg, thapsigargin; Tm, tunicamycin; UTR, untranslated region; VEGF, vascular endothelial growth factor; WAT, white adipose tissue; WT, wild-type; XBP1, X-box-binding protein 1.

translation of such mRNAs, which rely on alternative initiation mechanisms for their translation. However, there exists a gap in our understanding of how eIF2A functions in mammalian systems in vivo (on the organismal level) and ex vivo (in cells). Here, using an eIF2A-knockout (KO) mouse model, we present evidence implicating eIF2A in the biology of aging, metabolic syndrome and central tolerance. We discovered that eIF2A-KO mice have reduced life span and that eIF2A plays an important role in maintenance of lipid homeostasis, the control of glucose tolerance, insulin resistance and also reduces the abundance of B lymphocytes and dendritic cells in the thymic medulla of mice. We also show the eIF2A KO affects male and female mice differently, suggesting that eIF2A may affect sex-specific pathways. Interestingly, our experiments involving pharmacological induction of endoplasmic reticulum (ER) stress with tunicamycin did not reveal any substantial difference between the response to ER stress in eIF2A-KO and wild-type mice. The identification of eIF2A function in the development of metabolic syndrome bears promise for the further identification of specific eIF2A targets responsible for these changes.

KEYWORDS

ER stress, eukaryotic initiation factor 2A (eIF2A), life span, lipid homeostasis, metabolic syndrome

1 | INTRODUCTION

Messenger RNA (mRNA) translation is the final step of expression of genetic information and is commonly separated into four phases: initiation, elongation, termination and ribosome recycling.[1–3] Initiation of protein synthesis/translation in eukaryotes is a complex process requiring more than 12 different initiation factors.[1–6] Assembly of the 80S ribosome at the start codon within the majority of eukaryotic mRNAs involves binding of the mRNA 5′-m^{7}G cap structure to a group of proteins referred to as the cap-binding complex or eukaryotic initiation factor 4F (eIF4F), which consists of three proteins: eIF4E (the cap-binding protein), eIF4G (the scaffolding protein that bridges the mRNA and the ribosome), and eIF4A (the DEAD-box RNA-dependent ATPase/helicase).[3–6] This is followed by recruitment of the 40S ribosomal subunit and associated initiation factors (the 43S initiation complex comprising a 40S ribosomal subunit, initiation factors eIF1, eIF1A, eIF5, and eIF3 and an eIF2•GTP•Met-tRNAi ternary complex [TC]) to mRNA (via a bridge between eIF4G and the ribosome bound eIF3) and movement of the 43S initiation complex along the 5′-untranslated region in search of the initiation codon. This mechanism of translation initiation is broadly known as "ribosome scanning" and is believed to operate on the vast majority of eukaryotic mRNAs.[3–7] eIF2 is one of the key players in eukaryotic translation

initiation, and it is believed that under normal conditions eIF2 participates in the initiation of almost all cytoplasmic mRNAs in eukaryotic cells.[3–7] It appeared, however, that several other factors, and, specifically, eukaryotic initiation factor 2A (eIF2A),[8 (for a review)] Ligatin/eIF2D,[9,10] the complex of the oncogene product, MCT-1, and density regulated protein (DENR),[9] and eIF5B[11–13] can promote recruitment of methionyl-tRNAi (Met-tRNAi) to some 40S/mRNA complexes under conditions of inhibition of eIF2 activity (e.g., during the integrated stress response [ISR]) or eIF2 absence in a fully reconstituted translation initiation system. It is not clear, however, how the selection between these different factors that bind Met-tRNAi is achieved, and how their targets are identified by the cellular protein synthesis machinery. It is expected, however, that eIF2A, eIF2D, eIF5B, MCT-1/DENR likely have non-overlapping targets.[14]

eIF2A is a single subunit, 65-kDa protein that was first identified as a factor capable of stimulating Met-tRNAi binding to 40S ribosomal subunits in vitro.[15,16] However, in contrast to eIF2, which stimulates Met-tRNAi binding to 40S ribosomal subunits in a GTP-dependent manner, eIF2A did not reveal any GTP-dependence, but instead was found to direct binding of the Met-tRNAi to 40S ribosomal subunits in a codon-dependent manner.[15,16] Although eIF2A does not seem to function in major steps in the initiation process,[17,18]

it seems to be critical for a subset of minor initiation events such as re-initiation, internal initiation, or non-AUG initiation, which are important for translational control of specific mRNAs.[8 (for a review)]

The function of eIF2A in cellular physiology and human disease, has recently attracted substantial attention with the discovery of the eIF2A involvement in the control of antigen presentation by major histocompatibility complex (MHC) class I molecules,[14] the ISR[19] and tumor initiation and progression.[20] These experiments suggested a rather unique role of eIF2A in cellular physiology. We note, however, that these experiments utilized cellular systems, involving eIF2A silencing. Thus, there was a gap in our understanding of how eIF2A functions in mammalian systems in vivo (on the organismal level) and ex vivo/in vitro (in cells).

To fill in this gap, we created a homozygous eIF2A knockout (KO) mouse strain.[21] Initially, we found that the eIF2A-KO mice revealed no visible phenotype (at about 3–5 months of age), being similar in size and morphology to wild-type mice.[21] However, a more detailed analysis of these mice has shown that eIF2A affects a variety of physiological and pathophysiological processes. Importantly, we found that eIF2A-KO mice have decreased longevity in comparison with wild-type mice, therefore implicating eIF2A in the mechanisms of mortality and, potentially, the biology of aging. We also found that eIF2A KO affects male and female mice differently, suggesting that eIF2A may affect sex-specific/hormonal signaling pathways. In particular, we found that female eIF2A-KO mice reveal decreased longevity in comparison with both the eIF2A-KO male mice and wild-type mice. We provide further evidence showing that eIF2A may play an important role in the maintenance of lipid homeostasis and the development of metabolic syndrome in mice and that it is also involved in the control of glucose tolerance and insulin resistance. High-fat (HF) diet experiments exacerbated the development of metabolic syndrome in eIF2A-KO mice and additionally revealed sex-specific differences, showing that eIF2A-KO female mice fed on the HF diet exhibit a more pronounced (and significant) increase in body weight in comparison with eIF2A-KO male mice fed on HF diet. Additionally, our analysis of thymic B and dendritic cells in the thymic medulla reveals substantially altered central tolerance of the eIF2A-KO mice and compromised immune response. Central tolerance is a process that regulates immature B lymphocyte development to reduce the number of autoreactive cells recognizing self-antigens and is essential for proper immune cell functioning[22] and thus, eIF2A may potentially affect the genetic pathways that regulate tolerance. Collectively, these results demonstrate the involvement of eIF2A in the control of several important physiological processes in mammals.

2 | MATERIALS AND METHODS

2.1 | Ethical treatment of animals

All experimental procedures performed with animals in this study were approved by the Institutional Animal Care and Use Committee (IACUC) at Cleveland State University in accordance with NIH guidelines. Both wild-type and eIF2A-KO mice were on C57BL/6N background. Mice were randomly assigned and group cage housed with same-sex litter-mates in polycarbonate cages. Mice were allowed ad libitum access to food and water. A 5008 Formulab Diet (LabDiet, St. Louis, MO, USA, Cat# 5008), or an Adjusted Calories Diet (42% from Fat) (Envigo, Indianapolis, IN, USA, Cat# 88137) were used. Mice were on a standard 12-h light/12-h dark schedule, unless indicated otherwise.

2.2 | eIF2A-KO mouse

The generation of eIF2A-KO mouse has been described previously.[21] In brief, we have used the OmniBankII gene trap library containing mutated embryonic stem (ES) cell clones to generate the eIF2A-KO mouse. The ES cell clone IST13504C3 was identified from the library to contain a retroviral insertion (of a gene trap vector Omnibank Vector 74) in the eIF2A gene intron 1 (Figure S1). Insertion of the retroviral vector into the eIF2A gene (a single-copy gene in the mouse genome) leads to the splicing of the endogenous upstream exons into this cassette to produce a fusion that terminates further transcription of the eIF2A endogenous exons downstream of the insertion. The absence of eIF2A mRNA and protein expression was confirmed by RT-PCR and Western blotting with anti-eIF2A specific antibodies.

2.3 | Genotyping

Mice were screened prior to weaning at the age of 12–17 days. For genotyping, tail snip DNA was extracted using tail lysis procedure with Proteinase K as previously described.[21] PCR was performed to determine the presence of the gene trap using LongAmp™ Taq 2× Master Mix (New England Biolabs, Ipswich, MA, USA). The following pairs of primers were used to detect either the wild-type eIF2A gene F_{fwd}: 5′-GCCTTTCTTGAACTCTCACC-3′ and R_{rev}: 5′-GCAGACCACAGGTCACACAT-3′, giving rise to a 357 bp product and/or its disrupted variant F_{fwd}: 5′-GCCTTTCTTGAACTCTCACC-3′ and RV_{rev}: 5′-CCAAT AAACC CTCTT GCAGT TGC-3′ (216 bp product) as described previously.[21]

2.4 | Study design, animal weight and lifespan

Mice were observed on a daily basis and euthanized promptly when IACUC humane criteria were met, such as substantially diminished movement or motor activity, hunched posture, substantially reduced food intake, diarrhea, ocular exudates and piloerection. Date of mouse death was recorded when mice were found dead or unlikely to survive more than 24 h and therefore euthanized. Assessment of feeding behavior was done as follows: mice were provided with ad libitum amount of food prior to the start of the experiment. Mouse body weight measurements were performed starting at 4–5 weeks, and mouse weekly food consumption was measured starting at 16–17 weeks for an 8-week time period. All measurements were taken on the same day once per week between 10 and 11 a.m. For food consumption measurements, mice were housed in cages of 3–4 mice, and the average food consumption of the entire cage was used to generate the data. Tissues were collected at the end of 25–27 weeks, snap-frozen on dry ice and stored at −80°C until further analysis.

2.5 | Staining of tissue sections

Tissues were typically isolated from male and female mice at 25–27 weeks of age following lethal exposure to carbon dioxide and/or as indicated in the particular experiment. Thin slices of tissues were immediately fixed in acid methanol (60% methanol, 10% acetic acid, and 30% water). Paraffin-embedded sections (5 μm) underwent high-temperature antigen retrieval and paraffin removal in Trilogy (Cell Marque, Hot Springs, AR, USA) in a pressure cooker. Endogenous peroxidase activity was eliminated by incubation with 0.03% H_2O_2 for 10 min and nonspecific protein interactions inhibited by incubation with serum-free protein block (DAKO, Carpinteria, CA, USA). The slides were then stained using hematoxylin and eosin (H&E), and with the following primary antibodies: rat monoclonal anti-B220 (BD Bioscience, San Jose, CA, USA, Cat# ab214437) and rabbit polyclonal anti-CD11c (Synaptic Systems, Goettingen, Germany, Cat# 375 003). Primary antibodies were visualized using rat or rabbit on mouse HRP-Polymer Kits (Biocare Medical, Concord, CA, USA) followed by DAB (3,3′-Diaminobenzidine) staining and counterstained with hematoxylin. Slides were viewed by light microscopy, and images captured using ImagePro Plus (Media Cybernetics, Silver Springs, MD, USA). H&E staining was performed following standard procedures.[23]

2.6 | In-cage locomotor activity

Mice were fed their respective diets for at least 5 weeks before behavioral experiments were started. Single-caged mice were placed in their home cage and their in-cage locomotor activity was recorded using Power Analysis Software (PAS) Home Cage Photobeam System (San Diego Instruments, San Diego, CA, USA). Locomotor activity was continuously monitored and automatically recorded every 60 min for 72 h. Mouse locomotor activity was monitored under either a 12:12 h light/dark cycle, or a 24-h constant darkness. The data were analyzed using the PAS software.

2.7 | Blood glucose and glucose tolerance test

Mice in all diet groups were subjected to either a 16 h (overnight) or a 5 h (morning) fast prior to blood collection. Mice between 16–18 weeks were intraperitoneally injected with glucose (1 g/kg body weight) in PBS pH 7.4. Blood was collected via tail vein nick at indicated intervals and glucose levels measured using CVS Health Advanced Blood Glucose Meter and/or CVS Health Advanced Glucose Meter Test Strips (CVS, Woonsocket, RI, USA). Mice were allowed to recover one week between subsequent experiments.

2.8 | Insulin measurements and the insulin tolerance test

Mice in all diet groups were fasted for 5 h prior to blood collection. Mice between 16–18 weeks were intraperitoneally injected with insulin (0.35 μg/g body weight) in PBS pH 7.4. Blood was collected via tail vein nick at indicated intervals and glucose levels measured using CVS Health Advanced Blood Glucose Meter and/or CVS Health Advanced Glucose Meter Test Strips (CVS, Woonsocket, RI, USA).

Mouse blood serum insulin levels were measured in a fed-state, fasted state, and during glucose tolerance at the indicated timepoints using a commercially available Mouse Insulin ELISA Kit (Crystal Chem Inc, Elk Grove Village, IL, USA, Cat# 90080). Mice were allowed to recover one week between subsequent experiments.

2.9 | Pharmacological induction of ER stress with tunicamycin

Mice were intraperitoneally injected with 0.5 or 1 μg/g of a 0.1 mg/ml tunicamycin (Tm) solution (Tm from *Streptomyces* sp. (Sigma-Aldrich, St. Louis, MO, USA) dissolved in a sterile filtered 150 mM dextrose solution (150 mM dextrose in saline with 1% DMSO)) or a vehicle

solution (150 mM dextrose in saline with 1% DMSO) as previously described.[24] The lifespan as well as the daily weights of these animals were monitored for up to 7 days, after which the mice were euthanized via CO_2 followed by a cervical dislocation for a confirmation of euthanasia.

2.10 | Isolation and differentiation of primary preadipocytes

The primary preadipocytes were isolated as described previously[25] from 8–10 weeks old wild-type and eIF2A-KO male and female mice. The inguinal white adipose tissue (WAT) and the interscapular brown adipose tissue (BAT) were dissected and additional tissue and blood vessels were removed. The WAT and the BAT were digested with 1.5 U/ml Collagenase D (Roche, Indianapolis, IN, USA, Cat# 11088858001), Collagenase B (Roche, Indianapolis, IN, USA, Cat# 11088807001) and 2.4 U/ml Dispase II (Roche, Indianapolis, IN, USA, Cat# D4693) in PBS pH 7.4, supplemented with 10 mM $CaCl_2$ at 37°C in a shaking water bath at 200 strokes/minute until the solution became cloudy and most of the tissue was digested. Dulbecco's Modified Eagle Medium/Nutrient mixture F-12 GlutaMAX (DMEM/F12) (Life Technologies, Carlsbad, CA, USA, Cat# 10565018) supplemented with 8% FBS (Sigma Aldrich, St. Louis, MO, Cat #12303C), 50 U/ml penicillin and 50 μg/ml streptomycin (Thermo Fisher Scientific, Waltham, MA, USA, Cat# 15140148) were used for cell washing and separation through 100 μm and (subsequently) 70 μm cell strainers (Thermo Fisher Scientific, Waltham, MA, USA, Cat# 22363549 and Cat# 22363548). The filtered cell suspension was centrifuged at 1500 rpm for 5 min at room temperature. The cell pellet was then resuspended in growth media (DMEM/F12 supplemented with 15% FBS, 50 U/ml penicillin and 50 μg/ml streptomycin) and cells were plated on collagen I coated plates (Corning, NY, USA, Cat# 356401). Growth media was changed every other day until cells reached 70%–80% confluency. Cells were then subcultured at high density and induced to differentiate using 0.5 μg/ml insulin (Sigma Aldrich, St. Louis, MO, USA, Cat# I5523), 5 μM dexamethasone (Sigma Aldrich, St. Louis, MO, USA, Cat# D1756), 0.5 mM isobutylmethylxanthine (Sigma Aldrich, St. Louis, MO, USA, Cat# I5879) and 1 μM rosiglitazone (Cayman Chemical Company, Ann Arbor, MI, USA, Cat# 71740) in DMEM/F12 supplemented with 10% FBS, 50 U/ml penicillin and 50 μg/ml streptomycin. The media was switched to DMEM/F12 supplemented with 10% FBS, 50 U/ml penicillin and 50 μg/ml streptomycin, 0.5 μg/ml insulin after 2 days (Day 0). The cells were then analyzed on Day 4 for lipid accumulation and morphology at 10× magnification using the Olympus CKX53 microscope (Olympus Corporation, Tokyo, Japan).

2.11 | Oil red O staining of cultured cells

Oil Red O (ORO) staining of cultured cells was done following standard protocols.[26] ORO (Sigma Aldrich, St. Louis, MO, USA, Cat# O0625) was dissolved in isopropanol and filtered twice. The cells were fixed in freshly prepared 10% formalin for 10 min and washed with 60% Isopropanol, incubated with ORO stain for 10 min. Cells were then washed with water to remove the excess of stain. Upon drying, 100% isopropanol was added to elute the ORO. The absorbance was measured at 500 nm. Two tailed Student's t-test was used for statistical analysis of the data.

2.12 | Protein expression analysis

Total protein lysates were prepared from mouse tissues following standard procedures and analyzed using either the Proteome Profiling Adipokine Array Kit (R&D systems, Minneapolis, MN, USA, Cat# ARY013) and/ or Western blotting. The Proteome Profiling Adipokine Array Kit allows one to simultaneously detect the relative levels of 38 different obesity-related proteins in a single sample. The sample/antibody mixture was incubated on a pre-spotted nitrocellulose membrane, and relative expression of adipokines was measured following chemiluminescent detection of the signal using Odyssey Fc Imaging System (LI-COR Biosciences, Lincoln, NE, USA). Mice liver tissues (kept on dry ice) were disrupted using mortar and pestle and then lysed by sonication (5 s of sonication followed by 10 s on ice for a total of 3 cycles) in RIPA buffer (50 mM Tris-HCl pH 7.5, 150 mM NaCl, 2 mM EDTA, 1% NP40, 0.1% SDS, and 0.5% sodium deoxycholate) in the presence of Halt™ Protease Inhibitor Cocktail, EDTA-free (100×) (Thermo Fisher Scientific, Waltham, MA, USA, Cat# 78425) and Halt™ Phosphatase Inhibitor Cocktail (Thermo Fisher Scientific, Waltham, MA, USA, Cat# 78420). Lysates were clarified by centrifugation at 12 000 rpm for 20 min at 4°C. Adipose tissue lysates were prepared similarly except that they were kept on ice for 1 h after sonication for better separation of fat and then clarified by centrifugation as outlined in the previously described protocol.[27] The lysates' total protein content was quantified using the Pierce™ BCA Protein Assay Kit (Thermo Scientific, Cat# 23225). A total of 500 μg equivalents of samples for liver tissue and 1 mg equivalents of samples for adipose tissue were used for analysis with the Proteome Profiling Adipokine Array Kit. Data analyses were performed using the HLImage++ Array analysis software from Western Vision Software (Salt Lake City, UT, USA). Student's t-test was used for statistical analysis of the data. Western blotting was done following

standard procedures and using the following antibodies: anti-eIF2A (Abcam, MA, USA #ab169528) (1:2500); anti-eIF2α-P (Abcam, MA, USA #ab32157) (1:3000); anti-eIF2α (Santa Cruz Biotechnology, CA, USA #sc-133227) (1:3000); anti-PERK (Cell Signaling Technology, MA, USA #3192) (1:1000); anti-CHOP (Cell Signaling Technology, MA, USA #2895) (1:1000); anti-BiP (GRP 78) (Santa Cruz Biotechnology, CA, USA #sc-13968) (1:1000); anti-β-actin (Abcam, MA, USA #ab3280) (1:5000) and/or (Genetex, CA, USA #GTX629630) (1:1000), anti-PPARγ (Bethyl Laboratories, Inc, TX, USA #A304-460A) (1:10 000), anti-P62 (Proteintech, IL, USA #C827H23) (1:1000), anti-LC3B (Novus Biologicals, CO, USA #NB100-2220SS) (1:1000). Data were analyzed using Image Studio Lite software (LI-COR Biosciences, Lincoln, NE, USA). For Western blotting of mouse embryonic fibroblast cells (MEFs), MEFs were treated with DMSO and/or thapsigargin (Millipore-Sigma, Burlington, MA, USA #T9033) (400 nM) containing media for 16 h followed by cold PBS pH 7.4 wash (twice) and protein extraction. For protein extraction, cells were scraped off and lysed in lysis buffer (50 mM Tris-HCl, pH 7.5, 150 mM NaCl, 2 mM EDTA, 1% NP-40, 0.1% SDS and 0.5% sodium deoxycholate) supplemented with protease and phosphatase inhibitors (Roche, Indianapolis, IN, USA). Cell lysates were sonicated 10 rounds in 2 RMS on ice and centrifuged at 13 000 rpm for 10 min at 4°C. Supernatants were taken for protein quantification along with the protein lysates collected from mice tissues and equal amounts of protein (20 μg) were analyzed by SDS-PAGE and Western blotting following standard procedures.

2.13 | RT-PCR

Two-step SYBR real-time RT-PCR was performed. Total RNA was isolated from the cultured undifferentiated and differentiated (on day 4 post-differentiation) primary adipocytes isolated from WAT and BAT using Trizol-LS (Invitrogen, Carlsbad, CA, USA, Cat# 10-296-010) as described by the manufacturer. One μg of RNA was treated with RNase-free DNase-I (Thermo Scientific, Cat# EN0521) re-purified using Trizol-LS and further used for cDNA preparation with RevertAid First Strand cDNA Synthesis Kit (Thermo Scientific, Cat# K1621). The SYBR real-time RT-PCR was performed using the Power Up SYBR Green Master Mix (Applied Biosystems, Waltham, MA, USA, Cat# A25742) using the Bio-Rad (CFX Connect Real-Time PCR) detection system. C_t (cycle threshold) values were analyzed using the comparative C_t($\Delta\Delta C_t$) method. The amount of target p62 ($2^{-\Delta\Delta Ct}$) was obtained by normalization to an endogenous reference standard (β-actin) and relative to undifferentiated p62 levels. The following primers were

used: β-actin fwd: 5′-GCAGGAGTACGATGAGTCCG-3′, rev: 5′-ACGCAGCTCAGTAACAGTCC-3′; p62 fwd: 5′-TTGAAGTCTTTGGACCCCCG-3′, rev: 5′-CTCGAGT CACAGTGGACCCT-3′.

2.14 | Statistics and analysis

Data for all diets were analyzed using either one-way or two-way ANOVA. Post-hoc analysis was done using the Bonferroni′ method. The number of biological replicas used in each experiment is indicated in the Figure legends. Data is represented as Mean ± standard error of the mean. Statistical significance was set at $p \leq .05$ based on two tailed Student′s t-test.

3 | RESULTS

3.1 | eIF2A-KO mice reveal reduced life span

We have previously reported the construction and preliminary analysis of an eIF2A-KO mouse strain.[21] Our initial observation of 3–5 months old animals showed that the eIF2A null mice are viable and exhibit no visible abnormalities, being similar in size and morphology to wild-type mice under standard growth conditions.[21] However, our extended analysis (for more than a year) of the survival data showed that eIF2A-KO animals exhibit decreased survival rates. Statistical analyses of the mortality curves included calculation of Kaplan–Meier distributions of survival and comparison by a two-sided log rank test. We found that eIF2A-KO mice have substantially decreased probability of survival rates in comparison with wild-type (C57BL/6N) mice (Figure 1A). Decreased survival probability begins to manifest after about 3 months (90 days) of age. Furthermore, we found that eIF2A-KO female animals have lower survival probability in comparison with eIF2A-KO male animals (Figure 1A). Circadian clock and rhythms are important regulators of metabolism and longevity.[28] Increased mortality rates in mice can result from dissociation between the internal circadian rhythm (locomotor activity) and the external timing.[28] Therefore, we next tested if the locomotor activity and circadian rhythms of the eIF2A-KO mice had been affected.

3.2 | Locomotor activity and circadian rhythms of eIF2A-KO mice

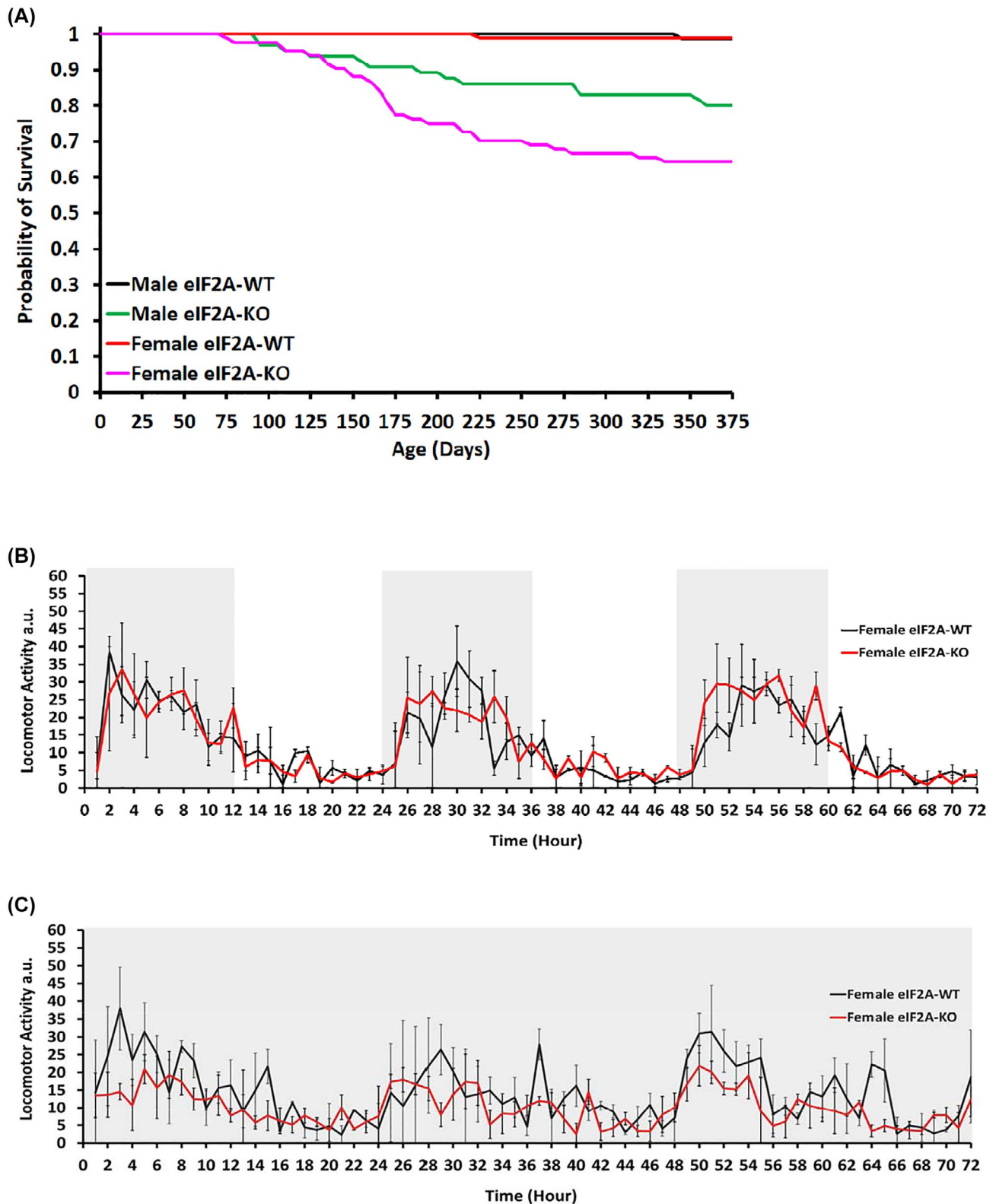We chose to analyze the daily and circadian rhythms of locomotor activity of eIF2A-KO female animals in

FIGURE 1 Survival of mice of the indicated genotypes and genders and assessment of behavior and locomotor activity. (A) Comparison of longevity group survival between WT (C57BL/6J) mice and eIF2A-KO mice (males and females monitored over 1 year) (Number of animals used for the analysis: WT Males = 83, eIF2A-KO Males = 65, WT Females = 85, eIF2A-KO Females = 84). (B) WT and eIF2A-KO female mice were placed in individual home cages, and their locomotion was assessed every hour for 72 h (with 12-h light and 12-h night [shaded grey] periods) ($n = 3$ for each group). (C) WT and eIF2A-KO female mice locomotion was assessed under constant darkness every hour for 72 h ($n = 3$ for each group)

comparison with wild-type female mice, since eIF2A-KO female animals reveal even lower survival rates than their male counterparts. Locomotor activity of eIF2A-KO female mice was continuously monitored and automatically recorded every 60 min for 72 h and compared to that of wild-type mice. eIF2A-KO and wild-type female mice ages between 170 and 195 days (when the difference in survival rates can be readily observed) were used. However, there were no significant differences between the eIF2A-KO and wild-type mice locomotor activity in a standard light/dark cycle (Figure 1B) or in constant darkness (Figure 1C). Thus, daily and circadian behavioral rhythms were not significantly affected by eIF2A deficiency. We have therefore concluded that the increased mortality and metabolic phenotype in eIF2A-KO mice were not likely due to the disruption of the circadian rhythms.

3.3 | Age-dependent obesity in eIF2A-KO mice

We were not able to observe any obvious/visible phenotypic differences between 3–5 months old eIF2A KO and wild-type animals.[21] However, we found that eIF2A-KO animals at one year of age (and older) display signs of severe obesity and hepatomegaly (enlarged liver) and also reveal extensive fat deposits in the abdominal cavity (Figure 2A,B). H&E staining further revealed substantial hepatic steatosis in eIF2A-KO, but not wild-type mice (Figure 2C), as well as increased adipocyte size in brown, gonadal and subcutaneous fat depots of eIF2A-KO mice (Figure 2D). Many factors influence body weight in C57BL/6 mice, and some of the strongest and well-known factors are age, sex and diet.[29] HF diet is widely used to induce obesity in mice.[30–32] Therefore, we next compared the effect of HF diet on wild-type and eIF2A-KO mice in young animals. The HF diet was introduced at 4 weeks of age in half of the animals, while the other half was maintained on the normal, low-fat diet. At this age, body weight was 14.3 ± 0.34 g in female wild-type mice and 13.8 ± 0.37 g for eIF2A-KO females and 16.5 ± 0.32 g in male wild-type mice and 14.8 ± 0.78 g for the eIF2A-KO males. As expected, after the introduction of the HF diet, body weight increased significantly more in the HF diet–fed mice than in the normal diet–fed mice (Figure 3A,B). However, the weight gain in eIF2A-KO mice was progressively higher than that in wild-type mice (Figure 3A,B). Furthermore, we found that eIF2A-KO female mice accumulated weight much faster than the eIF2A-KO male mice (Figure 3A,B). After 16–20 weeks of HF diet feeding, mice will typically exhibit 20%–30% increase in body weight when compared to normal diet–fed mice.[30] We found that eIF2A-KO female mice fed on the HF diet

exhibited a very substantial (76%) increase in body weight in comparison with eIF2A-KO female mice fed on normal diet (Figure 3). At the same time, wild-type female mice fed on the HF diet exhibited only about a 28% increase in body weight. The weight gain in eIF2A-KO male mice fed the HF diet was less pronounced (about 39%) in comparison with eIF2A-KO male mice fed on normal diet, yet it was more than that for wild-type male mice, which exhibit only about 25% increase in body weight when fed on the HF diet (Figure 3A,B).

3.4 | Daily food consumption is similar in wild-type and eIF2A-KO mice

The next logical question was whether eIF2A-KO mice display a different tendency to consume diet, as food intake is well known to be one of the factors affecting mammalian/mouse body weight.[33] For this purpose, we monitored food intake of eIF2A-KO and wild-type mice (16–17 weeks old male and female animals were used) for 8 weeks and compiled weekly food intake data. While both, eIF2A-KO and wild-type mice, showed some interindividual variability for food intake, we didn't find any statistically significant differences in food consumption between eIF2A-KO and wild-type animals, including both female and male mice (Figure 3C left panel—normal diet, right panel—HF diet). As expected, the food consumption was slightly reduced, when animals were fed on the HF diet, but again, we didn't find any statistically significant differences in food consumptions between eIF2A-KO and wild-type animals, including both female and male mice (Figure 3C, right panel).

3.5 | eIF2A-KO mice are in a prediabetic state

Increased adiposity has a strong relationship to diabetes and insulin resistance.[34] We found that 1-year old male eIF2A-KO animals (fed on a normal diet) display substantially reduced glucose tolerance as measured using intraperitoneal glucose tolerance test in comparison with WT mice. They also reveal marginally elevated basal/fasting glucose levels observed after overnight (16 h) fasting (Figure S2), suggesting signs of diabetes. Therefore, we next decided to check if signs of diabetic/pre-diabetic state can be found in younger animals. We found that under both mild (5 h) and extended (16 h) fasting conditions, the initial blood glucose levels were not significantly different between eIF2A-KO and wild-type 16–18 weeks old animals (Figure 4A,B). However, upon intraperitoneal glucose administration, we observed decreased glucose
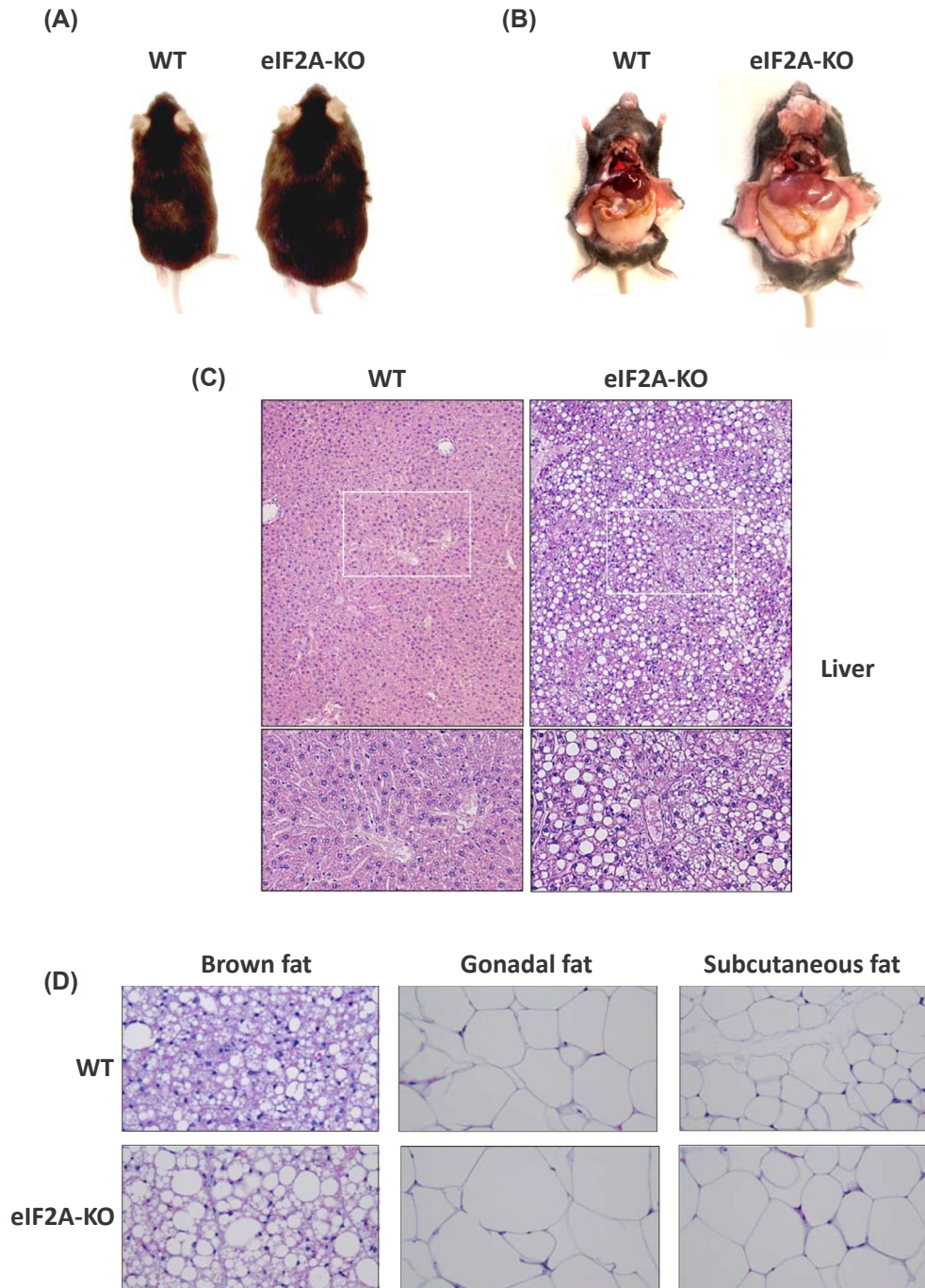
FIGURE 2 The eIF2A-KO mouse metabolic syndrome phenotype. (A) Representative photographs of 1 year old mice—WT (on the left) and with knockout of eIF2A gene (right). (B) Abdominal photograph of the same mice. Necropsies reveal extensive fat deposits in the abdominal cavity of eIF2A-KO, but not the wild-type mouse, completely encasing many organs. Enlarged fatty/steatotic liver can be also observed in case of eIF2A-KO mouse. (C) Hematoxylin and eosin (H&E) staining of paraffin embedded liver tissues from the same mice. H&E staining shows severe hepatic steatosis in eIF2A-KO mouse liver with large voids indicative of the fatty adipose deposits, but not in WT mice. Multifocal proliferation of lymphocytes in the liver of WT, but not the eIF2A-KO mice can be also observed. (D) H&E staining of adipose tissues (brown, gonadal and subcutaneous fat). H&E staining show increased size of adipocytes in eIF2A-KO mouse tissues (bottom panels), but not the WT mice (upper panels)

tolerance in both male and female mice, which was readily observed in experiments involving 5 h fasting conditions (Figure 4A,B, left panels) and were less significant or insignificant in experiments involving 16 h fasting conditions (Figure 4A,B, right panels). As expected, animals fed with the HF diet showed elevated glucose levels (Figure 4A,B) and under these conditions, the eIF2A-KO animals showed a more pronounced and similarly
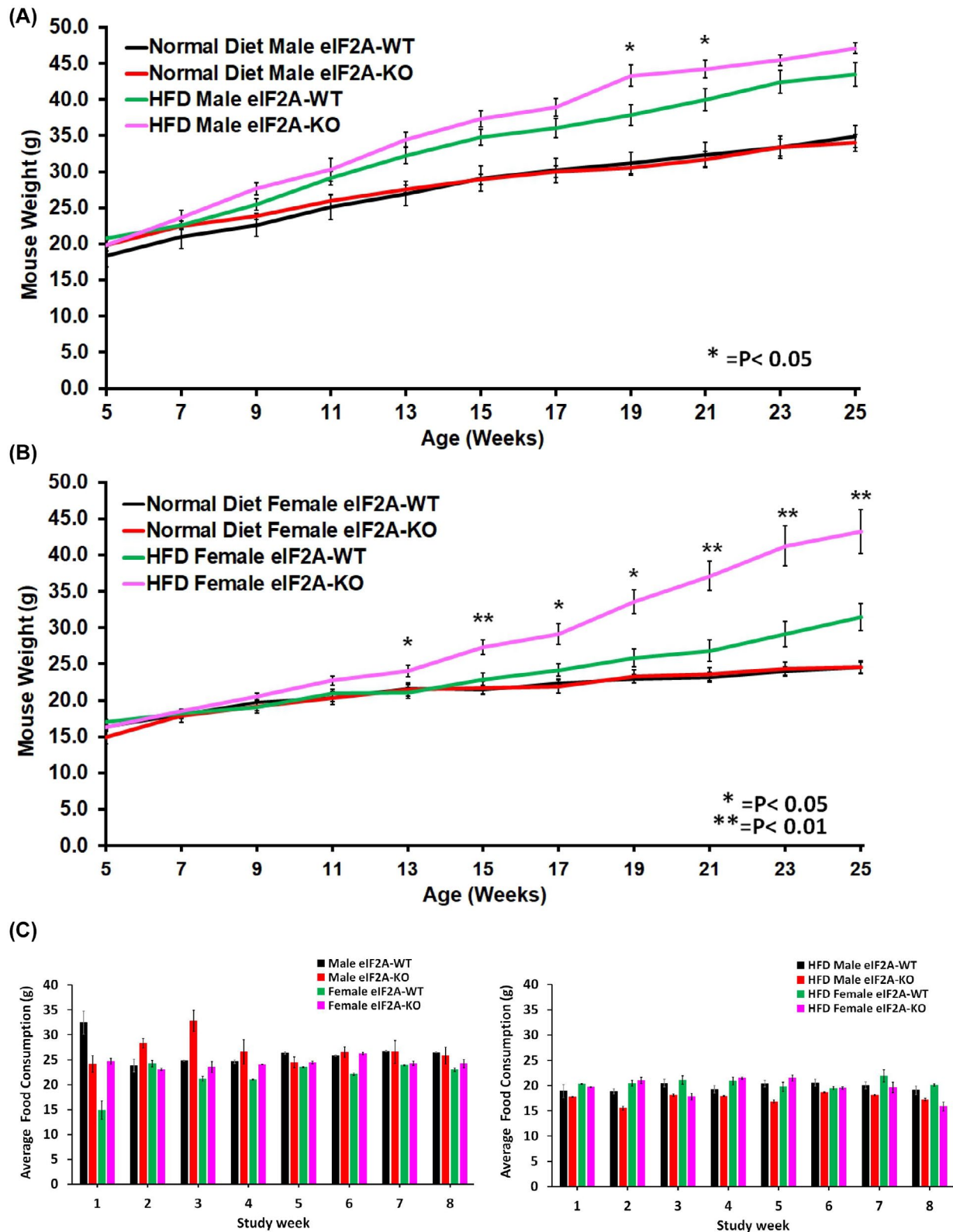
FIGURE 3 Mice body weight and food intake. (A) Change in body weight in male WT (C57BL/6J) and eIF2A-KO mice fed on normal and high-fat (HF) diets. (B) Change in body weight in female WT (C57BL/6J) and eIF2A-KO mice fed on normal and HF diets. All data presented as means ± SEM, $N = 8$ animals/group. $*p < .05$; $**p < .01$. (C) Weekly food intake. All data presented as means ± SEM, $N = 5–8$ animals/group
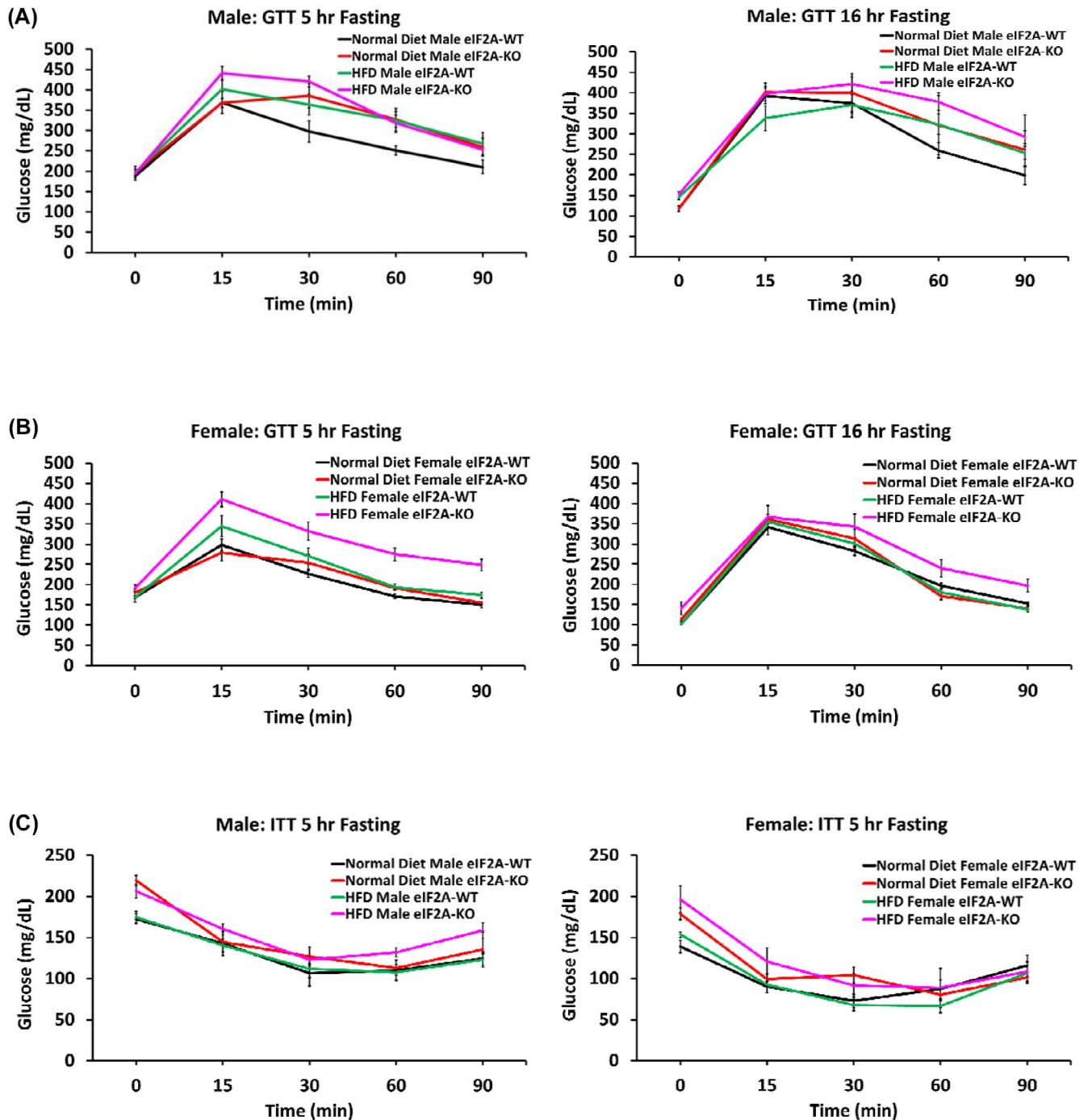
FIGURE 4 Plasma glucose concentrations during the intraperitoneal glucose tolerance (1 g/kg body weight) and insulin tolerance (0.35 µg/g body weight) tests in WT (C57BL/6J) and eIF2A-KO (16–18 weeks old) mice fed on normal and high-fat (HF) diets. (A) Intraperitoneal glucose tolerance test (GTT) in male mice following fasting for 5 h (left panels) and 16 h (right panels). (B) Intraperitoneal GTT in female mice following fasting for 5 h (left panels) and 16 h (right panels). (C) Insulin sensitivity. Male (left panel) and female (right panel) mice fed on normal and HF diets were fasted for 5 h and intraperitoneally injected with insulin. All data presented as means ± SEM, N = 5–8 animals/group

decreased glucose tolerance, which was again readily observed after 5-h fasting (Figure 4A,B left panels), but not after 16 h of fasting (Figure 4A,B, compare left and right panels). The difference in glucose tolerance was also more pronounced in eIF2A-KO female animals in comparison with male mice (Figure 4B, left panel). These experiments suggest that eIF2A-KO mice are in a prediabetic state. We next used an Intraperitoneal Insulin Tolerance Test to check for insulin resistance. We found that eIF2A-KO animals generally have moderately increased insulin

resistance (Figure 4C). This difference was again more pronounced in female eIF2A-KO animals (fed on HF diet) compared to wild-type animals (fed on the HF diet) (Figure 4C right panel). We also found that eIF2A-KO mice generally show a trend toward decreased insulin levels, which was more pronounced in 25–28 weeks animals in comparison with 16–18 weeks animals (Figure S3), suggesting that eIF2A may likely affect the function of the pancreatic beta cells.

3.6 | WAT and BAT differentiation ex vivo

To understand the reason for increased adiposity in eIF2A-KO mice, we isolated primary preadipocytes (from both the inguinal WAT and BAT) from 8–10 weeks old wild-type and eIF2A-KO male and female mice. Primary preadipocytes were sub-cultured at high density and induced to differentiate. The cells were analyzed on Day 4 (after induction of differentiation) for morphology and lipid accumulation using ORO staining. We found that eIF2A-KO WAT primary adipocytes reveal about ~69% increased ORO lipid staining in comparison with wild-type adipocytes upon differentiation in male (Figure 5A), but not female mice (Figure 5B). Interestingly, eIF2A-KO BAT primary adipocytes upon differentiation showed increased ORO lipid staining in both male (~64%) and female animals (~223%) (Figure 5C,D). These data reveal additional sex-specific difference between eIF2A-KO and WT mice.

3.7 | Adipokine profiling in mice tissues

Our analysis of key adipokine expression (using a Proteome Profiler Mouse Adipokine Array Kit) showed increased levels of lipocalin-2 in the liver (about 2-fold) and BAT (~1.5 fold) of eIF2A-KO mice in comparison with the wild-type animals (Figure 6A,B). Interestingly, we have also found almost 2-fold decrease in adiponectin

levels and nearly complete loss of insulin-like growth factor 2 in the BAT of eIF2A-KO mouse in comparison with the wild-type animals (Figure 6B). We also note that levels of several other important adipokines, known to regulate central tolerance and metabolism,[35] such as C-reactive protein, Intercellular Adhesion Molecule 1, Insulin-like growth factor-binding protein 2 (IGFBP-2), Insulin-like growth factor-binding protein 6 and Vascular endothelial growth factor (VEGF) appeared to be decreased in WAT of the eIF2A-KO mice in comparison with the wild-type animals (Figure 6B).
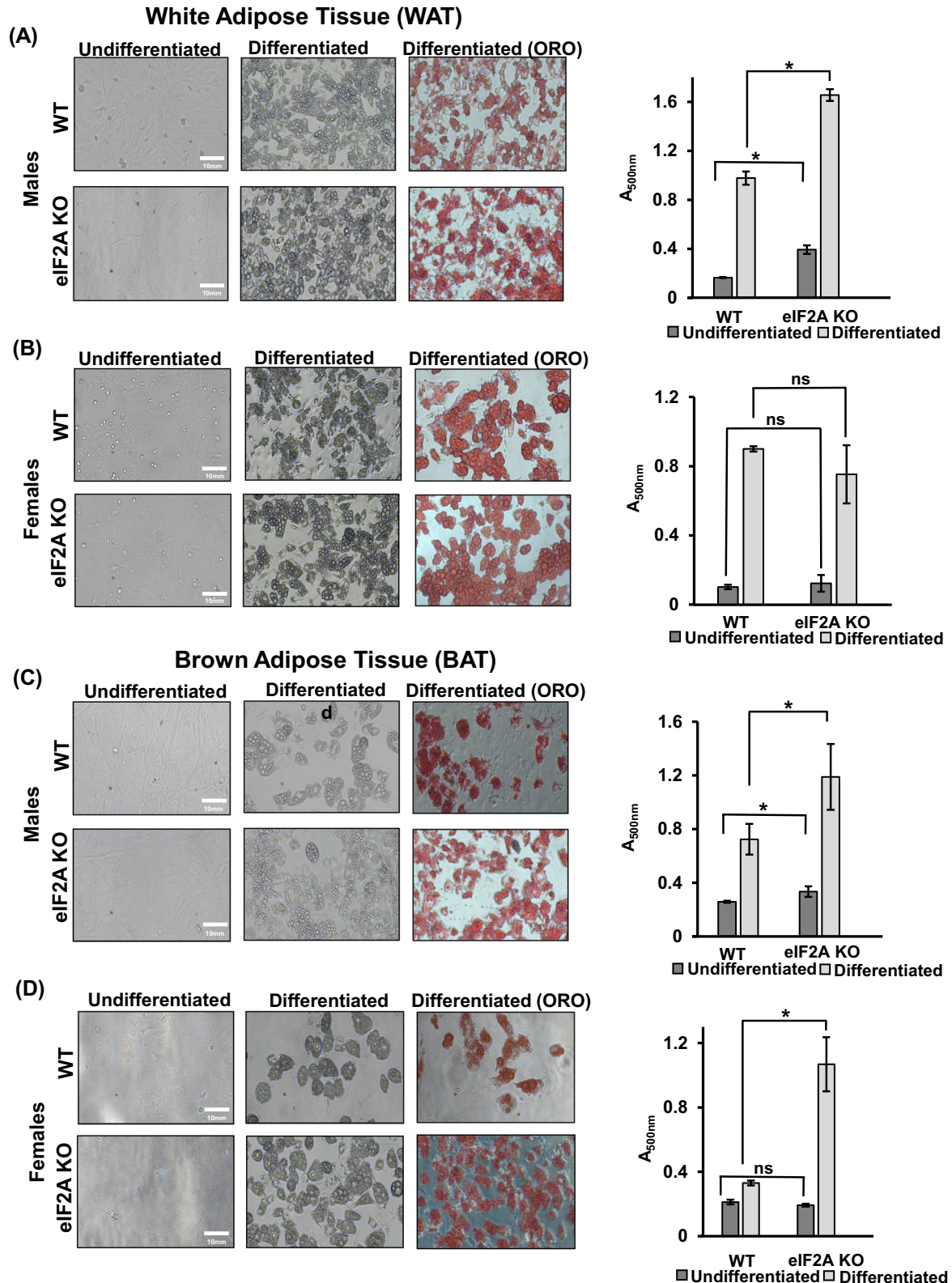
3.8 | Lysosomal lipolysis is likely compromised in eIF2A-KO mice

The lipid droplet is a dynamic organelle which is coated with proteins and which primarily regulates lipid flux.[36] Cytosolic lipolysis is mediated by a series of lipases including adipose triglyceride lipase, hormone-sensitive lipase, and monoacylglycerol lipase for triglycerides.[37] A major discovery in the field of lipolysis was the realization that autophagy is also utilized to catabolize lipids/lipid droplets, which are delivered as cargo to the lysosome.[38–40] In this process, the lipid droplet surface protein perilipin 2 (PLIN2) binds sequestosome-1 (SQSTM1/p62), a selective autophagy receptor, which in turn mediates interaction with microtubule associated protein 1 light chain 3 beta (LC3) on the autophagosomal surface to direct autophagosomes to the lipid droplets and thus, accelerate lipid turnover by lipophagy.[38–40] LC3 plays a central role in autophagosome membrane structure and exists in two forms: a cytosolic LC3-I (~19 kDa) form and a lipid modified form, known as LC3-II (~17 kDa), that is believed to be recruited for autophagosome membrane for expansion and fusion.[39] Detection of the conversion of LC3-I to LC3-II is also considered to be a useful autophagy marker.[41] Using primary WAT and BAT adipocytes we found that the absence of eIF2A in eIF2A-KO cells substantially reduces the induction of p62 (upon adipocyte

FIGURE 5 eIF2A affects lipid accumulation in primary adipocytes. (A) Standard primary adipocytes isolation and differentiation protocol were followed, and cells were stained with Oil Red O (ORO) at day 4 post-differentiation. (A) Primary preadipocytes isolated from White Adipose Tissue (WAT) of ~8-week-old male mice and induced for differentiation. Microscopy of undifferentiated, differentiated and ORO-stained cells is shown on the left. Quantitation of the staining results (absorbance at 500 nm is shown on the right; average of the three independent experiments utilizing tissues from 3 different mice). (B) Primary preadipocytes isolated from WAT of ~8-week-old female mice and induced for differentiation. Microscopy of undifferentiated, differentiated and ORO-stained cells (on the left). Quantitation of the staining results (absorbance at 500 nm is shown; average of the three independent experiments utilizing tissues from 3 different mice) (on the right). (C) Primary preadipocytes isolated from brown adipose tissue (BAT) of ~8-week-old male mice and induced for differentiation. Microscopy of undifferentiated, differentiated and ORO-stained cells (on the left). Quantitation of the staining results (absorbance at 500 nm is shown on the right; average of the 3 independent experiments utilizing tissues from 3 different mice). (D) Primary preadipocytes isolated from BAT of ~8 weeks old female mice and induced for differentiation. Microscopy of undifferentiated, differentiated and ORO-stained cells (on the left). Quantitation of the staining results (absorbance at 500 nm is shown; average of the 3 independent experiments utilizing tissues from 3 different mice) (on the right). *$p < .01$ (Student's t-test)

differentiation), but does not substantially affect the conversion of LC3-I to LC3-II (Figure 7A). However, the substantial reduction in p62 levels in differentiated cells may subsequently lead to the increased lipid accumulation observed in eIF2A-KO cells and may well explain increased ORO lipid staining in these cells. The induction of

expression of peroxisome proliferator-activated receptor γ (PPARγ)—a key regulator of adipocyte development both in vitro and in vivo[34,35] was used to confirm adipocyte differentiation (Figure 7A). We also note that the decrease in the induction of p62 protein levels is accompanied by a (moderate) decrease in the induction of p62 mRNA levels
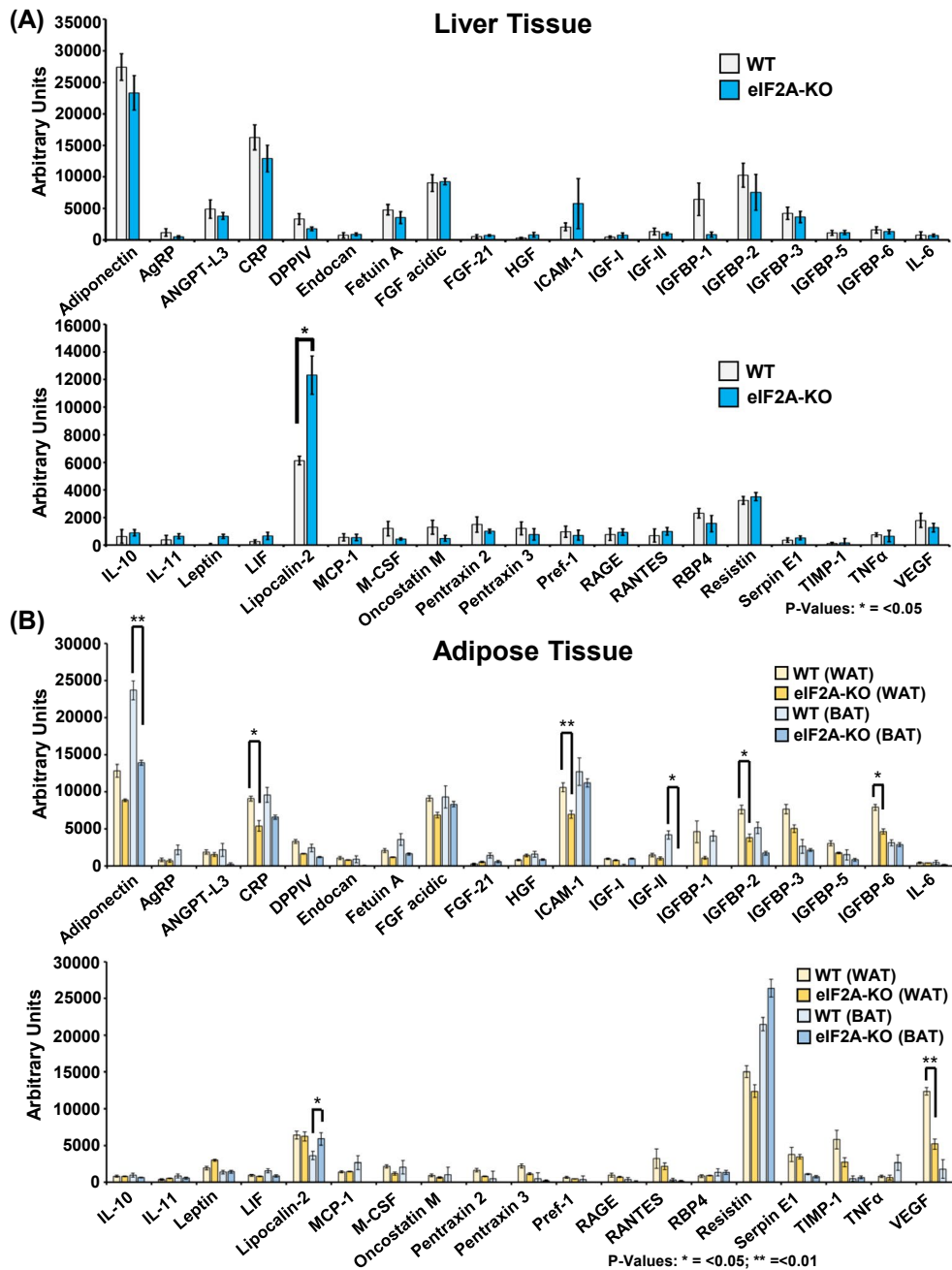

White Adipose Tissue (WAT)

(A) Males — WT / eIF2A KO — Undifferentiated, Differentiated, Differentiated (ORO)

(B) Females — WT / eIF2A KO — Undifferentiated, Differentiated, Differentiated (ORO)

Brown Adipose Tissue (BAT)

(C) Males — WT / eIF2A KO — Undifferentiated, Differentiated, Differentiated (ORO)

(D) Females — WT / eIF2A KO — Undifferentiated, Differentiated, Differentiated (ORO)

FIGURE 6 eIF2A affects adipokine expression in the liver and adipose tissue. (A) Analysis of adipokine expression in mice liver tissues. (B) Analysis of adipokine expression in mice WAT and BAT tissues. Mouse adipokine array with captured detection antibodies was incubated with tissue lysates followed by the chemiluminescent detection. Data analyses were done using the HLImage++ Array analysis software from Western Vision. Averages of the 3 independent experiments utilizing tissues from 3 different mice for liver tissue samples and from 4 different mice for adipose tissue samples are shown. Tissue samples were prepared as outlined in the materials and methods section. Two-tailed Student's t-test was used for calculating the p-values and statistical analysis of the data. p-values: *$< .05$; **$< .01$

in eIF2A-KO cells (Figure 7B). However, at present, it is not clear, whether this decrease in mRNA levels is sufficient to explain the observed decrease in p62 protein levels and/or that the decrease in p62 proteins levels may also stem from the inability of eIF2A to assist p62 translation in eIF2A-KO cells, or both. Further experiments will be required to determine whether eIF2A indeed controls the translation of p62 mRNA.

3.9 | Similar sensitivity of WT and eIF2A-KO mice in response to ER stress

eIF2A has been recently implicated in the ISR (invoked and investigated in several cellular models).[19,42,43] In particular, it was suggested that eIF2A may assist in the translation of the endoplasmic reticulum (ER) associated chaperone, binding immunoglobulin protein (BiP; also
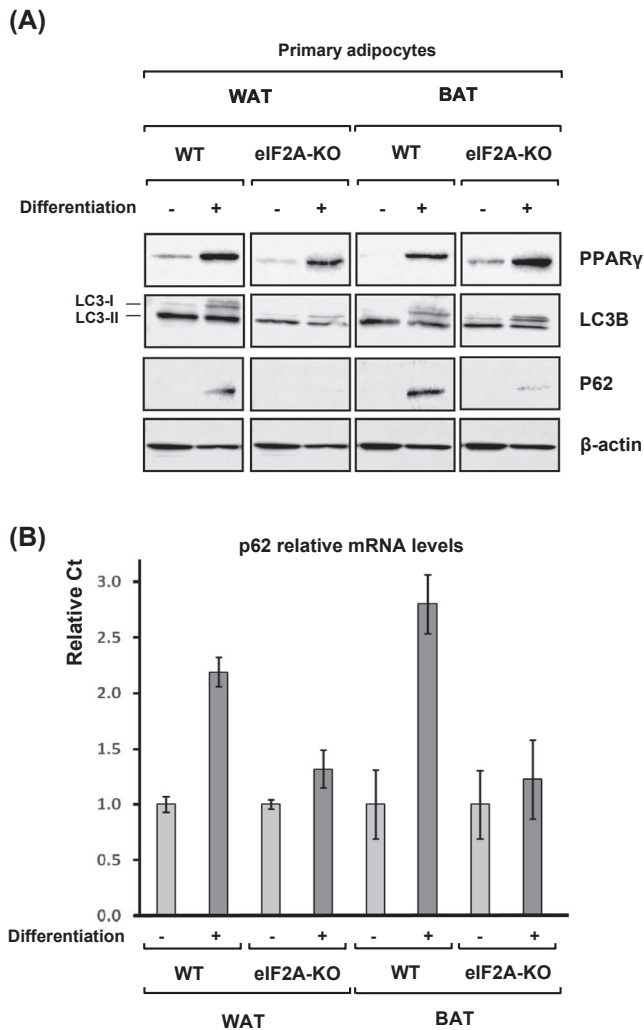
(A)

Primary adipocytes

(B)

FIGURE 7 eIF2A affects the expression levels of autophagic receptor, p62, in primary adipocytes upon differentiation. (A) Western blot of key adipogenic and autophagic markers: PPARγ, LC3B (represented by LC3-I (upper band) and LC3-II (lower band) isoforms) and p62 in wild-type and eIF2A-KO adipocytes isolated from WAT and BAT tissues before and after differentiation. (B) Real-time PCR. Relative C_t values are shown; C_t values were normalized to the actin signal and plotted relative to undifferentiated p62 mRNA levels. All data presented as means ± SEM, $N = 5$ independent points per each RT-PCR

known as Grp78)[19] during the ISR and help recovery from ISR. Tm is one of the most common agents used to study the effects of nucleoside antibiotics on protein folding and synthesis and associated ER/ISR stress. Tm alters hepatic energy homeostasis in mice,[44] triggers the rapid development of hepatic steatosis,[24,44] leads to decreased mouse weight and eventually may cause animal death.[24] Tm has been shown to cause premature death (after 2 days of administration) in ATF6α-KO mice by exacerbating the effects of ER stress in these animals.[24] We therefore tested the effect of Tm on wild-type and eIF2A-KO mice. Mice were intraperitoneally injected with either 0.5 or 1 µg/g of

a 0.1 mg/ml Tm (dissolved in 150 mM dextrose in saline with 1% DMSO) and/or a vehicle solution (150 mM dextrose in saline with 1% DMSO) and monitored for up to 7 days after the injection. The lifespan, daily weights, liver pathology (at the end of the experiment) and the expression of the key ISR markers (in the liver samples) were assessed. Surprisingly, we didn't observe substantial differences between the life span and the body weight of wild-type mice and eIF2A-KO mice (both males and females) after Tm injection (Figure 8A). Both wild-type and eIF2A-KO animals (both males and females) were progressively losing weight after Tm injections, albeit with similar trends (Figure 8A). Predictably, the weight loss was more severe after using a higher (1 µg/g) concentration of Tm, however, even under these conditions, no statistically significant differences between wild-type mice and eIF2A-KO mice were observed (Figure 8A middle panel). We note, however, that in the latter case we had to terminate this experiment earlier (around 5–6 days from the start) in order to prevent mice suffering from significant pain and distress and/or due to the occasional mouse death. Consistent with the discolored appearance of the liver and the development of hepatic steatosis (Figure 8B), we observed induction of lipid droplet formation in the livers of both wild-type and eIF2A-KO (Figure 8C). However, again no substantial difference between the liver morphology and/or pathology between the wild-type and eIF2A-KO mice were observed.

The liver is a major site for the production of the many secretory/plasma proteins and the ER stress is a key player in regulating their synthesis and maturation.[45] Under normal circumstances/non-stress conditions, the ER chaperone BiP (Grp78), binds the N-termini of inositol-requiring enzyme 1 (IRE1), PKR-like ER kinase (PERK), and activating transcription factor 6 (ATF6), thus preventing their activation.[46,47] Misfolding and aggregation of ER-resident proteins redirects BiP towards these new targets and causes it to release IRE1, PERK, and ATF6, resulting in the activation of the former proteins and in turn launching a cascade of downstream signaling events.[46,47] Activation of PERK through its oligomerization and autophosphorylation results in phosphorylation of eIF2α and downregulation of general protein synthesis. This in turn launches a cascade of events in particular leading to activation of transcription of the CCAAT enhancer binding protein homologous protein (CHOP), which plays a critical role in ER stress-mediated apoptosis and in diseases like diabetes, as well as induction of other factors that help restoring protein synthesis.[46,47] Predictably, we found that Tm treatment leads to the activation of PERK via its autophosphorylation, which in turn led to increased phosphorylation of eIF2α and the induction of BiP as one of the key markers of ER stress (Figure 8D). However, we didn't observe any substantial difference between wild-type mice and eIF2A-KO
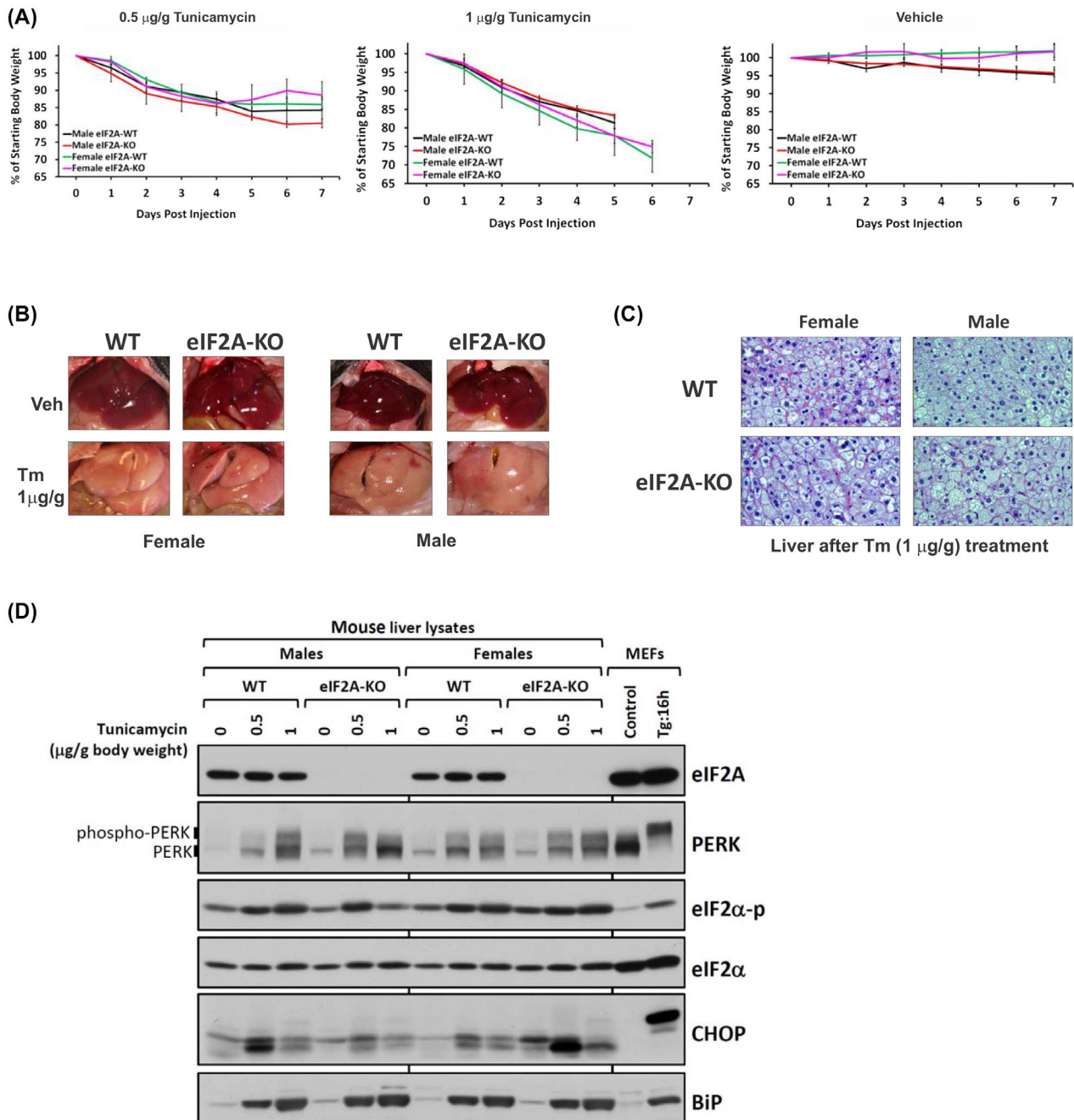
FIGURE 8 eIF2A does not alter the response to Endoplasmic Reticulum stress caused by intraperitoneal injections of tunicamycin (Tm): effect of Tm injection on mice body weight, liver appearance and integrated stress response markers. (A) Tm was intraperitoneally injected into WT (C57BL/6J) and eIF2A-KO mice each at a dose of 0.5 μg/g (left panel) or 1 μg/g body weight (middle panel), respectively. Vehicle solution (150 mM dextrose in saline with 1% DMSO) was used as a control (right panel). Body weights of injected mice were determined daily for 7 days and are presented after normalization to that at day 0 of injection as the means ± SEM (N = 3–4 for Tm-injected mice and N = 3–4 for others). In order to prevent mice suffering from significant pain and distress and/or due to occasional mice death measurements of body weight in case of 1 μg/g Tm were terminated earlier. (B) Liver photographs (the abdomen of injected mice was dissected at the end of the experiment). (C) Hematoxylin and Eosin (H&E) staining of paraffin embedded liver tissues from Tm injected mice. H&E staining shows severe hepatic steatosis in both WT and eIF2A-KO mouse. (D) Western blotting analysis for the key ISR markers of liver samples and/or mouse embryonic fibroblasts (MEFs) treated or not treated with Tm and/or thapsigargin (Tg)

mice (both males and females) in terms of the levels of induction of all these proteins (Figure 8D). The higher (1 μg/g) Tm concentration led to a more extensive induction

of BiP, phospho-PERK and phospho-eIF2α, but again no differences between wild-type mice and eIF2A-KO mice were observed. Surprisingly, we found that CHOP levels

were already quite high even without the Tm treatment in the liver of all the animals tested (Figure 8D). These results contrast with those observed for MEFs, where induction of ER stress, predictably has led to a strong induction of the all the key ISR markers including CHOP (Figure 8D). These results suggest that additional factors may be present in vivo that modulate the observed differences. However, we have concluded that the absence of eIF2A doesn't exacerbate the effects of ER stress in eIF2A-KO mice.

3.10 | Altered immune tolerance in eIF2A-KO mouse

Obesity impairs immune function and alters cell-mediated immune responses.[34,35] Therefore, we examined whether there were signs of altered immune tolerance in eIF2A-KO mice in comparison with the wild-type animals. B220, also known as isoform of cluster of differentiation 45 (CD45) protein (CD45R) is a member of the protein tyrosine phosphatase family and is predominantly expressed on B lymphocytes, including pro-, matured and activated B cells and such serves as B lymphocytes marker.[48-50] We specifically looked at the medulla of the thymus, which is specialized for promoting tolerance against autoantigens expressed in peripheral tissues.[51] We found that the expression of the B220 antigen was substantially reduced in thymic medulla of eIF2A-KO mice in comparison with wild-type mice (Figure 9A, left panel). We also found that the CD11c antigen (a type I transmembrane protein, known also as integrin alpha X), which is abundantly expressed in monocytes/dendritic cells and
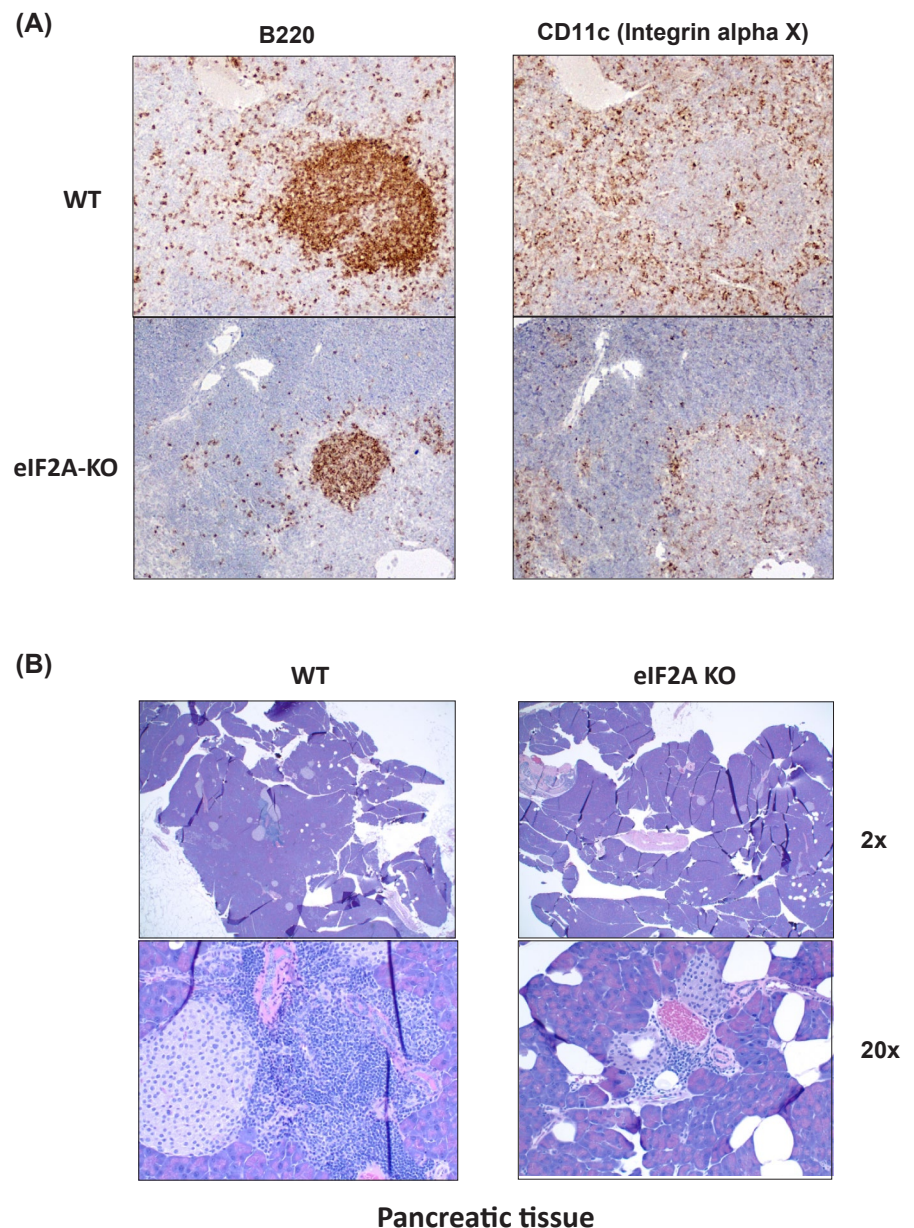

FIGURE 9 Altered immune tolerance in eIF2A-KO mouse. (A) Immunostaining of the thymic medulla samples from WT and eIF2A-KO mice using anti-B220 antibodies (B220 is a marker of B lymphocytes) and anti-CD11c antibodies (CD11c, a type I transmembrane protein, known also as integrin alpha X is a marker of monocytes/dendritic cells). (B) Hematoxylin and eosin (H&E) staining of paraffin embedded pancreatic tissues. H&E staining shows substantial multifocal proliferation of lymphocytes in tissues of WT, but not the eIF2A-KO mice

macrophages,[52] also showed decreased expression in thymic medulla of eIF2A-KO mice in comparison with wild-type mice (Figure 9A, right panel). Additionally, we observed decreased proliferation of lymphocytes in both pancreas (Figure 9B) and liver (Figure S4) of eIF2A-KO mice in comparison with wild-type mice (this difference can be observed as early as in three-month-old animals). Interestingly, lymphocytic aggregates were mostly observed next to islands of Langerhans in eIF2A-KO mice (Figure 9B). Together these data suggest that eIF2A-KO mice possess altered immune tolerance. However, further experiments would be necessary to understand the exact mechanism(s) behind the observed changes.

4 | DISCUSSION

The eIF2A protein homologues have been found in a wide range of eukaryotic species from yeast to mammals, suggesting a conserved biological role for this factor.[8] However, the precise role of eIF2A, as well as the precise mechanism of its action remain enigmatic. Cellular studies implicated eIF2A in minor initiation pathways that affect the translation of only a subset of mRNAs, such as internal ribosome entry site-containing mRNAs and/or mRNAs harboring upstream near cognate/non-AUG start codons (like e.g., CUG, GUG, UUG).[8 (for a review)] These non-canonical initiation events were suggested to be important for regulation of protein synthesis during cellular development and/or the ISR.[53] Selective eIF2A knockdown in cellular systems has been shown to significantly inhibit CUG-initiated, but not AUG-initiated events and affect such processes like antigen presentation by MHC class I molecules,[14] the ISR[19] and tumor initiation and progression[20] that were suggested to rely on such alternative initiation mechanisms.

There is yet a substantial gap in our understanding of how eIF2A functions ex vivo (in mammalian cells) and in vivo in animal models. Recently, we developed an eIF2A-total body KO mouse model and initiated its preliminary characterization.[21] Here, we present a more in-depth analysis of these mice. Unexpectedly, we found that eIF2A-KO mice had decreased longevity in comparison with the wild-type mice (Figure 1A). We also found that female eIF2A-KO mice have an even lower longevity in comparison with both the eIF2A-KO male mice and wild-type mice (Figure 1A). The exact reason for the decreased longevity in the eIF2A-KO animals is unknown, and as can be seen from the discussion below, there might be multiple reasons for such an abnormality, rather than one single reason. In general, laboratory mice strains are known to have different median lifespans ranging from about 250 to 960 days.[54] Median lifespans of C57BL family members

range from 866 days (in female mice) to 901 days (in male mice).[54] The sex differences do not significantly affect lifespan in laboratory mice[54] and our findings that female eIF2A-KO mice have lower longevity in comparison with the eIF2A-KO male mice suggests that eIF2A may affect sex-specific signaling pathways. Accumulating data do reveal sex specific difference in several signaling pathways (such as e.g., TGF-β-signaling[55]) and suggest, for example, that diabetes may be associated with an imbalance in sex hormone levels, but it has not yet been conclusively clarified how the levels of testosterone and/or estrogen and their respective receptors and the imbalance between them are exactly related to the differences in disease progression in both sexes.[56,57]

We also examined if locomotor activity and daily/circadian rhythms of locomotor activity were affected in eIF2A-KO mice. Locomotor activity and circadian rhythms of locomotor activity are important indicators of health.[28] Decreased locomotor activity and weak circadian activity rhythms are known to bear higher mortality risks.[28] However, our analysis of daily and circadian rhythms of locomotor activity didn't reveal any substantial difference between eIF2A-KO mice in comparison with wild-type animals (Figure 1B,C). We have therefore concluded that eIF2A loss doesn't substantially affect circadian and locomotor activity in mice and next performed gross and pathology examination of selected tissues and organs of the eIF2A-KO mice (Figure 2). We didn't find any substantial difference between, brain, heart and lungs of the eIF2A-KO mice compared to the wild-type animals (not shown), however we found that eIF2A-KO mice display typical signs of metabolic syndrome,[58,59] revealing enlarged steatotic liver (full of lipid droplets), increased abdominal obesity, and increased adipocyte size in brown, gonadal and subcutaneous fat (Figure 2). These changes appeared to be exacerbated with the age of the mice. These results suggested an altered mouse physiology upon eIF2A loss, which may have influenced the synthesis and degradation of lipids in eIF2A-KO mice and/or feeding behavior to alter overall metabolism.

Foods that are rich in fats have been widely used in animal/mouse models to exacerbate the development of metabolic abnormalities that otherwise may be developed slowly in the life of the animals.[30–33] Our experiments showed that eIF2A-KO mice fed on a HF diet gain significantly more weight in comparison with the wild-type animals. Interestingly, the eIF2A-KO female mice fed on the HF diet exhibited a more pronounced (and significant) increase in body weight in comparison with eIF2A-KO male mice fed on the HF diet (Figure 3), therefore further suggesting that eIF2A may affect sex-specific/hormonal pathways regulating metabolism. We note, however, that we didn't find any statistically significant differences in

food consumptions between eIF2A-KO and wild-type animals, suggesting that the metabolic syndrome phenotype observed in these animals doesn't stem from increased food consumption (Figure 3C), but is likely caused by the defects in lipophagy and moderately increased insulin resistance (see below).

The metabolic syndrome phenotype seems to have three main etiological categories: obesity and disorders of adipose tissue; glucose intolerance and insulin resistance; and a constellation of independent factors (such as abnormal expression of molecules of hepatic, vascular, and immunologic origin) that mediate specific components of the metabolic syndrome.[58,59] Our analysis of eIF2A-KO animals revealed decreased glucose tolerance in both male and female mice and increased insulin resistance, which was exacerbated by the HF diet (Figure 4). The difference in glucose tolerance was also more pronounced in eIF2A-KO female animals in comparison with male mice and is exacerbated with the age of the animals (Figure S2). In addition, we found that eIF2A-KO mice generally displayed decreased insulin levels; this difference was more pronounced in 25 to 28-week-old animals in comparison with 16 to 18-week-old animals (Figure S3). These results suggest that eIF2A may likely affect the function of the pancreatic beta cells. We also note that overall insulin levels were lower in female than male mice (both eIF2A-KO and wild-type). We have therefore concluded that eIF2A-KO mice display the typical signs of a prediabetic state.

To further understand the reason for increased adiposity in eIF2A-KO mice, we isolated primary preadipocytes (from both the inguinal WAT and BAT) and assessed their ability to accumulate lipids upon differentiation. Adipose tissue plays a central role in the regulation of energy balance and homeostasis.[35] There are two main types of adipose tissue, WAT and BAT.[60] It is widely accepted that the main function of WAT is to store excess energy in the form of triacylglycerols, whereas the main function of BAT is to dissipate energy as heat.[60] We found that eIF2A-KO primary adipocytes generally reveal increased ORO lipid staining in comparison with wild-type adipocytes upon differentiation (Figure 5). This difference was more pronounced in eIF2A-KO BAT primary adipocytes than in WAT primary adipocytes (Figure 5C,D). Hence, we have concluded that eIF2A directly or indirectly affects lipid metabolism.

Lipogenesis is known to be affected by both internal and external stimuli, such as e.g., insulin, which induce the ERK1/2 signaling pathway leading to activation of enzymes such as ATP citrate lyase, acetyl-CoA carboxylase, fatty acid synthase and others.[61] A number of other external stimuli (except insulin) are known to affect lipogenesis.[61] These include but are not limited to such hormones

as leptin, lipocalin-2 (LCN2), also known as oncogene 24p3 or neutrophil gelatinase-associated lipocalin protein, and/or growth hormones.[61] Interestingly we have found increased levels of lipocalin-2 in the liver (about 2-fold) and BAT (~1.5-fold) of eIF2A-KO mice in comparison with the wild-type animals (Figure 6A,B). Lcn2 has been implicated in the apoptotic induction of pro-B cells and has been suggested to promote insulin resistance in adipocytes.[62] Lipocalin-2 levels were also reported to be increased in obese individuals[63] and elevated LCN2 levels were observed in obese mice models as well.[64] We have also found an almost 2-fold decrease in adiponectin levels in BAT of eIF2A-KO mouse in comparison with the wild-type animals (Figure 6B). Adiponectin modulates a number of metabolic processes, including glucose regulation and fatty acid oxidation and its levels are known to be inversely correlated with body mass index.[65] Additionally, levels of several other important adipokines, known to regulate central tolerance and metabolism were affected. These observations further allowed us to conclude that eIF2A broadly affects lipid metabolism.

It must be noted that intracellular lipid metabolism is a complex interplay of lipid trafficking, storage, lipolysis, and export.[36–40] Using primary WAT and BAT adipocytes, we found that the absence of eIF2A in eIF2A-KO cells substantially reduces the induction (upon differentiation) of p62 (Figure 7A), a selective autophagy receptor, which mediates an interaction of perilipin 2 (PLIN2) on the lipid droplets with microtubule associated protein 1 LC3 on the autophagic membrane to direct sequestration of lipid droplets inside the forming autophagosomes and thus, accelerate lipid turnover by lipophagy.[37–40] Substantial reduction in p62 levels are consistent with the increased lipid accumulation observed in eIF2A-KO cells, however, whether eIF2A affects p62 expression directly or indirectly remains to be established, as the decrease in the induction of p62 protein levels was also accompanied by a decrease in the induction of p62 mRNA levels in eIF2A-KO cells (Figure 7B).

Eukaryotic cells, when exposed to a variety of stress conditions, activate the so-called ISR to restore homeostasis. In mammals, four stress-activated kinases[66] (PKR-like ER kinase (PERK), double-stranded RNA-dependent protein kinase (PKR), heme-regulated eIF2α kinase (HRI), and general control non-derepressible 2 (GCN2)) reduce the level of active eIF2 by phosphorylating the eIF2α subunit and, consequently, reducing the global level of translation.[3–7,66] Phosphorylation of the α subunit of the eIF2 complex inhibits eIF2B-mediated exchange of eIF2-GDP to eIF2-GTP, thus reducing the formation of the active TC.[3–7,66] However, translation of a subset of mRNAs appears to be resistant to eIF2α phosphorylation, despite requiring Met-tRNAi. eIF2A, in particular, has been

implicated in the ISR and suggested to assist in the translation of the ER associated chaperone, BiP and thus, help recovery from ISR.[19] However, our experiments which involved pharmacological induction of ER stress with Tm in mice didn't reveal any substantial difference between the response to ER stress in eIF2A-KO and wild-type mice (Figure 8). Both, pathological changes associated with the Tm administration and the induction of the key ER-stress markers (phospo-PERK, eIF2α-P, BiP, CHOP) remain very similar (practically, identical) between the eIF2A-KO and wild-type mice (Figure 8). We have, therefore, concluded that in the context of the animal model, eIF2A doesn't modulate the expression of BiP and the absence of eIF2A doesn't exacerbate the effects of ISR in eIF2A-KO mice, in contrast to a well-known ATF6α-KO mice model, that are unable to recover from the insult caused by Tm treatment.[24] When burdened with the intraperitoneal injection of Tm, the ATF6α-KO mice exhibited an inability to efficiently induce BiP, displayed much more severe liver dysfunction and steatosis in comparison with wild-type mice and eventually died (2 days from the start of Tm (1 μg/g) administration).[24]

Obesity is known to impair the immune function, altering leukocyte counts as well as cell-mediated immune responses.[34,35] Our analysis of the medulla of the thymus of the eIF2A-KO mice revealed altered central tolerance in comparison with the wild-type animals as observed by the decrease in the expression of B lymphocytes and monocytes/dendritic cells (Figure 9A). We also found decreased proliferation of lymphocytes in both pancreas (Figure 9B) and liver (Figures 2C and S4) of eIF2A-KO mice in comparison with wild-type mice. Together these data strongly indicate that eIF2A-KO mice also possess altered immune tolerance. However, an understanding of the exact mechanism(s) underlying altered immune tolerance in eIF2A-KO mice is as yet lacking.

Emerging findings indicate that the translational control of gene expression plays important role in the preservation of cellular homeostasis and the development of several disease states.[67–71] Specifically, translational control was shown to be required for maintenance of in vivo glucose homeostasis.[68,72] Mice with a mutation at the eIF2α phosphorylation site (Ser51Ala) died within 18 h after birth due to hypoglycemia associated with defective gluconeogenesis.[72] It was also found that eIF2α mice mutant embryos and neonates display a deficiency in pancreatic beta cells and altered hepatocyte function due to their inability to attenuate translation under ER stress. eIF2α (Ser51Ala) mutation also led to about 2-fold decrease in IGFBP-2 and VEGF levels[72] (in addition to alteration in expression of many other signaling molecules) similarly

to what we observed in eIF2A-KO mouse, therefore suggesting that eIF2 and eIF2A might have (direct or indirect) overlapping targets. It is becoming apparent that translational control may also play a central role in lipid metabolic processing and storage pathways.[73–77] Interestingly, it was recently shown that eIF4E-deficient mice demonstrate defects completely opposite to what we observed in eIF2A-KO mice.[77] Upon HF diet feeding, $eIF4E^{+/−}$ mice appeared to be resistant to diet-induced obesity; they also display increased glucose tolerance and reduced lipid accumulation (in the liver) in comparison with the wild-type mice. Curiously, PLIN2 expression appeared to be elevated in $eIF4E^{+/−}$ mice upon HF diet feeding, therefore resulting in enhanced lipid processing.[77] The authors concluded that the reduction in eIF4E levels protects mice from the diet-induced obesity, enhancing optimal lipid processing.[77] Previously, mice mutant for eIF4E binding/inhibitor proteins—eIF4E-binding proteins 1 and 2 (4EBP1/2) have been shown to have altered adipogenesis and circulating leptin levels, resulting in increased feeding and obesity phenotypes.[73–77] Using yeast as a model system, we have previously shown that eIF4E and eIF2A genetically interact and function in the same pathway and thus likely may share similar targets.[18] Last but not least, it was recently shown that eIF4G1, the scaffolding protein that binds eIF4E and eIF4A to form the cap-binding complex, eIF4F, is critical for beta cell function and glucose homeostasis.[78] Beta-cell specific eIF4G1-KO mice displayed glucose intolerance and deficits in insulin secretion.[78] Altogether these data demonstrate an essential role for the translational control as well as specific initiation factors in glucose homeostasis, beta cell function and lipid metabolism. We thus believe that the identification of specific eIF2A function in the development of obesity and metabolic syndrome adds to our understanding of these processes and bears promise for further identification of specific and direct eIF2A targets, responsible for these changes. However, whether e.g., p62 and/or adiponectin represent direct or indirect eIF2A targets remain to be established.

In summary, in this manuscript, we have evaluated the profound influence of the deletion of eIF2A in the KO mouse. Clearly, changes in the life span and the development of metabolic syndrome in the eIF2A-KO mice were especially clear. However, it is entirely possible that more subtle changes may be uncovered with more definitive examination of the mouse's response to both development and stress. An initial indication of this was seen in the altered immune tolerance although the mechanism is currently uncertain. More refined examination of the mouse anatomy and the physical behavior of these animals will constitute studies for the future.

ORCID
Anton A. Komar https://orcid.org/0000-0003-4188-0633

REFERENCES
1. Ramakrishnan V. Ribosome structure and the mechanism of translation. *Cell*. 2002;108:557-572.
2. Schmeing TM, Ramakrishnan V. What recent ribosome structures have revealed about the mechanism of translation. *Nature*. 2009;461:1234-1242.
3. Jackson RJ, Hellen CU, Pestova TV. The mechanism of eukaryotic translation initiation and principles of its regulation. *Nat Rev Mol Cell Biol*. 2010;11:113-127.
4. Voigts-Hoffmann F, Klinge S, Ban N. Structural insights into eukaryotic ribosomes and the initiation of translation. *Curr Opin Struct Biol*. 2012;22:768-777.
5. Hinnebusch AG. The scanning mechanism of eukaryotic translation initiation. *Annu Rev Biochem*. 2014;83:779-812.
6. Hinnebusch AG, Ivanov IP, Sonenberg N. Translational control by 5′-untranslated regions of eukaryotic mRNAs. *Science*. 2016;352:1413-1416.
7. Pelletier J, Sonenberg N. The organizing principles of eukaryotic ribosome recruitment. *Annu Rev Biochem*. 2019;88:307-335.
8. Komar AA, Merrick WC. A retrospective on eIF2A-and not the alpha subunit of eIF2. *Int J Mol Sci*. 2020;21:2054.
9. Skabkin MA, Skabkina OV, Dhote V, Komar AA, Hellen CU, Pestova TV. Activities of ligatin and MCT-1/DENR in eukaryotic translation initiation and ribosomal recycling. *Genes Dev*. 2010;24:1787-1801.
10. Dmitriev SE, Terenin IM, Andreev DE, et al. GTP-independent tRNA delivery to the ribosomal P-site by a novel eukaryotic translation factor. *J Biol Chem*. 2010;285:26779-26787.
11. Choi SK, Lee JH, Zoll WL, Merrick WC, Dever TE. Promotion of met-tRNAiMet binding to ribosomes by yIF2, a bacterial IF2 homolog in yeast. *Science*. 1998;280:1757-1760.
12. Pestova TV, de Breyne S, Pisarev AV, Abaeva IS, Hellen CU. eIF2-dependent and eIF2-independent modes of initiation on the CSFV IRES: a common role of domain II. *EMBO J*. 2008;27:1060-1072.
13. Terenin IM, Dmitriev SE, Andreev DE, Shatsky IN. Eukaryotic translation initiation machinery can operate in a bacterial-like mode without eIF2. *Nat Struct Mol Biol*. 2008;15:836-841.
14. Starck SR, Jiang V, Pavon-Eternod M, et al. Leucine-tRNA initiates at CUG start codons for protein synthesis and presentation by MHC class I. *Science*. 2012;336:1719-1723.
15. Merrick WC, Anderson WF. Purification and characterization of homogeneous protein synthesis initiation factor M1 from rabbit reticulocytes. *J Biol Chem*. 1975;250:1197-1206.
16. Adams SL, Safer B, Anderson WF, Merrick WC. Eukaryotic initiation complex formation. Evidence for two distinct pathways. *J Biol Chem*. 1975;250:9083-9089.
17. Zoll WL, Horton LE, Komar AA, Hensold JO, Merrick WC. Characterization of mammalian eIF2A and identification of the yeast homolog. *J Biol Chem*. 2002;277:37079-37087.
18. Komar AA, Gross SR, Barth-Baus D, et al. Novel characteristics of the biological properties of the yeast *Saccharomyces cerevisiae* eukaryotic initiation factor 2A. *J Biol Chem*. 2005;280:15601-15611.
19. Starck SR, Tsai JC, Chen K, et al. Translation from the 5′ untranslated region shapes the integrated stress response. *Science*. 2016;351:aad3867.
20. Sendoel A, Dunn JG, Rodriguez EH, et al. Translation from unconventional 5′ start sites drives tumour initiation. *Nature*. 2017;541:494-499.
21. Golovko A, Kojukhov A, Guan BJ, et al. The eIF2A knockout mouse. *Cell Cycle*. 2016;15:3115-3120.
22. Yamano T, Nedjic J, Hinterberger M, et al. Thymic B cells are licensed to present self antigens for central T cell tolerance induction. *Immunity*. 2015;42:1048-1061.
23. Feldman AT, Wolfe D. Tissue processing and hematoxylin and eosin staining. *Methods Mol Biol*. 2014;1180:31-43.
24. Yamamoto K, Takahara K, Oyadomari S, et al. Induction of liver steatosis and lipid droplet formation in ATF6alpha-knockout mice burdened with pharmacological endoplasmic reticulum stress. *Mol Biol Cell*. 2010;21:2975-2986.
25. Yu H, Emont M, Jun H, Wu J. Isolation and differentiation of murine primary brown/beige preadipocytes. *Methods Mol Biol*. 2018;1773:273-282.
26. Kraus NA, Ehebauer F, Zapp B, Rudolphi B, Kraus BJ, Kraus D. Quantitative assessment of adipocyte differentiation in cell culture. *Adipocyte*. 2016;5:351-358.
27. Diaz Marin R, Crespo-Garcia S, Wilson AM, Sapieha P. RELi protocol: optimization for protein extraction from white, brown and beige adipose tissues. *MethodsX*. 2019;6:918-928.
28. Valentinuzzi VS, Scarbrough K, Takahashi JS, Turek FW. Effects of aging on the circadian rhythm of wheel-running activity in C57BL/6 mice. *Am J Physiol*. 1997;273:R1957-R1964.

29. Nishikawa S, Yasoshima A, Doi K, Nakayama H, Uetsuka K. Involvement of sex, strain and age factors in high fat diet-induced obesity in C57BL/6J and BALB/cA mice. *Exp Anim.* 2007;56:263-272.

30. Speakman J, Hambly C, Mitchell S, Krol E. Animal models of obesity. *Obes Rev.* 2007;8(suppl 1):55-61.

31. Wang CY, Liao JK. A mouse model of diet-induced obesity and insulin resistance. *Methods Mol Biol.* 2012;821:421-433.

32. Heydemann A. An overview of murine high fat diet as a model for type 2 diabetes mellitus. *J Diabetes Res.* 2016;2016:2902351.

33. Ellacott KL, Morton GJ, Woods SC, Tso P, Schwartz MW. Assessment of feeding behavior in laboratory mice. *Cell Metab.* 2010;12:10-17.

34. Ghaben AL, Scherer PE. Adipogenesis and metabolic health. *Nat Rev Mol Cell Biol.* 2019;20:242-258.

35. Ouchi N, Parker JL, Lugus JJ, Walsh K. Adipokines in inflammation and metabolic disease. *Nat Rev Immunol.* 2011;11:85-97.

36. Olzmann JA, Carvalho P. Dynamics and functions of lipid droplets. *Nat Rev Mol Cell Biol.* 2019;20:137-155.

37. Young SG, Zechner R. Biochemistry and pathophysiology of intravascular and intracellular lipolysis. *Genes Dev.* 2013;27:459-484.

38. Singh R, Kaushik S, Wang Y, et al. Autophagy regulates lipid metabolism. *Nature.* 2009;458:1131-1135.

39. Zhang X, Evans TD, Jeong SJ, Razani B. Classical and alternative roles for autophagy in lipid metabolism. *Curr Opin Lipidol.* 2018;29:203-211.

40. Rahman MA, Kumar R, Sanchez E, Nazarko TY. Lipid droplets and their autophagic turnover via the raft-like vacuolar nicrodomains. *Int J Mol Sci.* 2021;22:8144.

41. McLeland CB, Rodriguez J, Stern ST. Autophagy monitoring assay: qualitative analysis of MAP LC3-I to II conversion by immunoblot. *Methods Mol Biol.* 2011;697:199-206.

42. Sonobe Y, Ghadge G, Masaki K, Sendoel A, Fuchs E, Roos RP. Translation of dipeptide repeat proteins from the C9ORF72 expanded repeat is associated with cellular stress. *Neurobiol Dis.* 2018;116:155-165.

43. Chen L, He J, Zhou J, et al. EIF2A promotes cell survival during paclitaxel treatment *in vitro* and *in vivo*. *J Cell Mol Med.* 2019;23:6060-6071.

44. Feng B, Huang X, Jiang D, Hua L, Zhuo Y, Wu D. Endoplasmic reticulum stress inducer tunicamycin alters hepatic energy homeostasis in mice. *Int J Mol Sci.* 2017;18:1710.

45. Kuscuoglu D, Janciauskiene S, Hamesch K, Haybaeck J, Trautwein C, Strnad P. Liver - master and servant of serum proteome. *J Hepatol.* 2018;69:512-524.

46. Ron D, Walter P. Signal integration in the endoplasmic reticulum unfolded protein response. *Nat Rev Mol Cell Biol.* 2007;8:519-529.

47. Hetz C, Zhang K, Kaufman RJ. Mechanisms, regulation and functions of the unfolded protein response. *Nat Rev Mol Cell Biol.* 2020;21:421-438.

48. Coffman RL. Surface antigen expression and immunoglobulin gene rearrangement during mouse pre-B cell development. *Immunol Rev.* 1982;69:5-23.

49. Hardy RR, Carmack CE, Shinton SA, Kemp JD, Hayakawa K. Resolution and characterization of pro-B and pre-pro-B cell stages in normal mouse bone marrow. *J Exp Med.* 1991;173:1213-1225.

50. Hathcock KS, Hirano H, Murakami S, Hodes RJ. CD45 expression by B cells. Expression of different CD45 isoforms by subpopulations of activated B cells. *J Immunol.* 1992;149:2286-2294.

51. Thapa P, Farber DL. The role of the thymus in the immune response. *Thorac Surg Clin.* 2019;29:123-131.

52. Poltorak MP, Schraml BU. Fate mapping of dendritic cells. *Front Immunol.* 2015;6:199.

53. Kearse MG, Wilusz JE. Non-AUG translation: a new start for protein synthesis in eukaryotes. *Genes Dev.* 2017;31:1717-1731.

54. Yuan R, Tsaih SW, Petkova SB, et al. Aging in inbred strains of mice: study design and interim report on median lifespans and circulating IGF1 levels. *Aging Cell.* 2009;8(3):277-287.

55. Ziller N, Kotolloshi R, Esmaeili M, et al. Sex differences in diabetes- and TGF-β1-induced renal damage. *Cells.* 2020;9:2236.

56. Maric C. Sex, diabetes and the kidney. *Am J Physiol Ren Physiol.* 2009;296:680-688.

57. Kautzky-Willer A, Harreiter J, Pacini G. Sex and gender differences in risk, pathophysiology and complications of type 2 diabetes mellitus. *Endocr Rev.* 2016;37:278-316.

58. Cornier MA, Dabelea D, Hernandez TL, et al. The metabolic syndrome. *Endocr Rev.* 2008;29:777-822.

59. O'Neill S, O'Driscoll L. Metabolic syndrome: a closer look at the growing epidemic and its associated pathologies. *Obes Rev.* 2015;16:1-12.

60. Lo KA, Sun L. Turning WAT into BAT: a review on regulators controlling the browning of white adipocytes. *Biosci Rep.* 2013;33:e00065.

61. Holm C, Osterlund T, Laurell H, Contreras JA. Molecular mechanisms regulating hormone-sensitive lipase and lipolysis. *Annu Rev Nutr.* 2000;20:365-393.

62. Devireddy LR, Teodoro JG, Richard FA, Green MR. Induction of apoptosis by a secreted lipocalin that is transcriptionally regulated by IL-3 deprivation. *Science.* 2001;293:829-834.

63. Catalán V, Gómez-Ambrosi J, Rodríguez A, et al. Increased adipose tissue expression of lipocalin-2 in obesity is related to inflammation and matrix metalloproteinase-2 and metalloproteinase-9 activities in humans. *J Mol Med.* 2009;87:803-813.

64. Yan QW, Yang Q, Mody N, et al. The adipokine lipocalin 2 is regulated by obesity and promotes insulin resistance. *Diabetes.* 2007;56:2533-2540.

65. Stern JH, Rutkowski JM, Scherer PE. Adiponectin, leptin, and fatty acids in the maintenance of metabolic homeostasis through adipose tissue crosstalk. *Cell Metab.* 2016;23:770-784.

66. Donnelly N, Gorman AM, Gupta S, Samali A. The eIF2α kinases: their structures and functions. *Cell Mol Life Sci.* 2013;70:3493-3511.

67. Le Quesne JP, Spriggs KA, Bushell M, Willis AE. Dysregulation of protein synthesis and disease. *J Pathol.* 2010;220:140-151.

68. Volchuk A, Ron D. The endoplasmic reticulum stress response in the pancreatic β-cell. *Diabetes Obes Metab.* 2010;12:48-57.

69. Piccirillo CA, Bjur E, Topisirovic I, Sonenberg N, Larsson O. Translational control of immune responses: from transcripts to translatomes. *Nat Immunol.* 2014;15:503-511.

70. Chu J, Cargnello M, Topisirovic I, Pelletier J. Translation initiation factors: reprogramming protein synthesis in cancer. *Trends Cell Biol.* 2016;26:918-933.

71. Robichaud N, Sonenberg N. Translational control and the cancer cell response to stress. *Curr Opin Cell Biol.* 2017;45:102-109.

72. Scheuner D, Song B, McEwen E, et al. Translational control is required for the unfolded protein response and *in vivo* glucose homeostasis. *Mol Cell.* 2001;7:1165-1176.

73. Tsukiyama-Kohara K, Poulin F, Kohara M, et al. Adipose tissue reduction in mice lacking the translational inhibitor 4E-BP1. *Nat Med*. 2001;7:1128-1132.

74. Le Bacquer O, Petroulakis E, Paglialunga S, et al. Elevated sensitivity to diet-induced obesity and insulin resistance in mice lacking 4E-BP1 and 4E-BP2. *J Clin Invest*. 2007;117: 387-396.

75. Le Bacquer O, Combe K, Montaurier C, et al. Muscle metabolic alterations induced by genetic ablation of 4E-BP1 and 4E-BP2 in response to diet-induced obesity. *Mol Nutr Food Res*. 2017;61(9):1700128.

76. Pearl D, Katsumura S, Amiri M, et al. 4E-BP-dependent translational control of *Irf8* mediates adipose tissue macrophage inflammatory response. *J Immunol*. 2020;204:2392-2400.

77. Conn CS, Yang H, Tom HJ, et al. The major cap-binding protein eIF4E regulates lipid homeostasis and diet-induced obesity. *Nat Metab*. 2021;3:244-257.

78. Jo S, Lockridge A, Mohan R, et al. Translational factor eIF4G1 regulates glucose homeostasis and pancreatic β-cell function. *Diabetes*. 2021;70:155-170.

SUPPORTING INFORMATION

Additional supporting information may be found in the online version of the article at the publisher's website.